HCR
Humans and Chemical Regimes
HCR 2(1): 41–71
ISSN 3048-393X

Institute for Advanced Science, Social and Sustainable Future
MORALITY BEFORE KNOWLEDGE

Eco-intelligent integrated pre-fenton and artificial neural network system for debottlenecking the efficiency of physico-chemical treatment in POP-B3 waste management

Naufal Fawwaz Dienulloh[1,*], Rizky Maulana Riadhi[1], Supriyono[1]
[1] *Department of Chemical Engineering, Faculty of Engineering, Universitas Brawijaya, Malang, East Java, 65145, Indonesia.*
*Correspondence: naufalfawwaz@student.ub.ac.id

Received Date: January 20, 2025 Revised Date: February 25, 2025 Accepted Date: February 28, 2025

ABSTRACT

Background: Persistent Organic Pollutants (POPs) in hazardous waste (B3) continue to increase due to industrial activities and are difficult to degrade using conventional methods. POPs can accumulate in the environment and pose serious health risks, such as cancer and reproductive disorders. The PREC-Fenton system has been proposed to enhance the treatment efficiency of hazardous waste, particularly POPs, by combining chemical reactions with energy utilization from salinity gradient power. **Methods**: The research methodology comprises modeling approaches, research framework formulation, system definition, thermodynamic property regression, model construction, system simulation, financial feasibility study, and simulation result analysis. **Findings:** The research findings indicate that the PREC-Fenton system is capable of reducing POPs by up to 1,038.8 kg/h with an efficiency of 99.99%, while producing 176.24 kg/h of clean water and generating 300.17 kW of energy with a conversion efficiency of 40%. The integration with the ORC system increased the energy efficiency to 46.13%. System optimization using an Artificial Neural Network (ANN) with 13 neurons in a single hidden layer yielded the lowest RMSE values and high accuracy, with R^2 values exceeding 0.96 for the K_P, K_I, and K_D parameters. The economic analysis showed a break-even point (BEP) at 44% capacity, a net present value (NPV) of USD 125,529, an internal rate of return (IRR) of 33.48%, and discounted payback period (DPP) of 5 years. These results confirm that the PREC-Fenton system is efficient, cost-effective, and environmentally friendly. **Conclusion**: This study successfully developed an efficient PREC-Fenton system for hazardous waste (B3) treatment, achieving up to 99.99% degradation efficiency of POPs, clean water production of 176.24 kg/h, and energy generation of 300.17 kW. **Novelty/Originality of this article:** This article presents an innovative integration of the PREC-Fenton system with an adaptive control approach based on Artificial Neural Networks (ANN) to optimize the real-time degradation of POP-B3 waste.

KEYWORDS: artificial neural network; hazardous waste (B3); persistent organic pollutants (pops); pid controller; prec-fenton.

1. Introduction

Persistent Organic Pollutants (POPs) are hazardous chemical compounds recognized by the World Health Organization (WHO) and the US Environmental Protection Agency (US EPA) for their environmental persistence, bioaccumulation potential, and severe health and ecological risks. These compounds exhibit high environmental persistence and strong lipophilicity, making them resistant to natural degradation processes and prone to bioaccumulation in the fatty tissues of living organisms (Pizzorno & Murray, 2021). Their

Cite This Article:
Dienulloh, N. F., Riadhi, R. M., & Supriyono. (2025). Eco-intelligent integrated pre-fenton and artificial neural network system for debottlenecking the efficiency of physico-chemical treatment in POP-B3 waste management. *Humans and Chemical Regimes, 2*(1), 41-71. https://doi.org/10.61511/hcr.v2i1.2043

ability to travel long distances through atmospheric and oceanic pathways has led to their detection even in remote regions such as Antarctica, where no direct industrial activities exist (Kim et al., 2024). The accumulation of POPs has been closely associated with adverse health effects, including cancer, immune dysfunction, reproductive issues, and developmental risks in fetuses and newborns (Rokni et al., 2023). In Indonesia, rapid industrial growth paired with poor hazardous waste management has escalated POP-containing waste release, posing a severe public health and environmental crisis (Xu et al., 2021). In response, international initiatives like the Stockholm Convention have been introduced to regulate the production, use, and emissions of POPs globally.

Despite these regulatory efforts, existing waste treatment technologies remain inadequate for effectively removing POPs (Matesun et al., 2024). Conventional industrial and physical treatment systems fail to degrade these stable pollutants, often only redistributing them to other environmental compartments without neutralizing their toxicity (Dapaah et al., 2022; Hassan et al., 2020). Advanced techniques such as Microbial Fuel Cells and ionizing radiation have been explored but are hindered by high costs and moderate operational efficiency, particularly at large scales (Balogun et al., 2020; Moallemi et al., 2020). Similarly, bioremediation-based alternatives, including microbial fuel cells, constructed wetlands, and genetic manipulation, although eco-friendly and adaptable to both aerobic and anaerobic conditions, suffer from slow pollutant removal rates, toxic byproduct formation, and high maintenance demands (Hassan et al., 2024; Hariram et al., 2023). This situation highlights the urgent need for more efficient, adaptable, and sustainable treatment solutions capable of degrading POPs while supporting broader environmental objectives (Eisenmenger et al., 2020).

One of the most promising alternatives is the Fenton-based Advanced Oxidation Process (AOP), which utilizes hydroxyl radicals (•OH) generated from hydrogen peroxide (H_2O_2) and ferrous ions (Fe^{2+}) to rapidly oxidize and degrade organic pollutants (Rokni et al., 2023), The reaction proceeds as follows (Jiménez-Bambague et al., 2023):

$$Fe^{2+} + H_2O_2 \rightarrow Fe^{3+} + \cdot OH + OH^- \quad \text{(Eq. 1)}$$

While effective, conventional Fenton systems face challenges in operational stability under dynamic conditions (Machado et al., 2023). To overcome these, Photocatalytic Reverse Electrodylisis Cell (PREC) Fenton system was developed by integrating salinity gradients that accelerate hydroxyl radical generation, thereby enhancing degradation efficiency while enabling concurrent renewable energy production (Hariram et al., 2023; Eisenmenger et al., 2020). This innovation combines Photocatalytic Fuel Cell (PFC) and Reverse Electrodialysis (RED) technologies, where PFC removes pollutants from wastewater while simultaneously recovering electrical energy and RED exploits salinity gradients to produce additional current (Dubowski et al., 2024; Hajiali et al., 2022).

The Reverse Electrodialysis (RED) system integrated within the PREC-Fenton process utilizes ammonium bicarbonate (NH_4HCO_3) solutions due to their ability to readily dissociate into NH_4^+ and HCO_3^-/CO_3^{2-} ions, which are essential for establishing a stable electrochemical gradient (Tian & Wang, 2022). In this setup, a concentrated NH_4HCO_3 solution functions as the ion donor, while a diluted NH_4HCO_3 solution acts as the ion acceptor (Leng et al., 2024). The difference in ion concentration drives the migration of cations and anions through selective membranes (Cation Exchange Membranes (CEM) and Anion Exchange Membranes (AEM)) from high to low concentrations, generating an electrical potential (Thakur & Malmali, 2022). This potential is subsequently converted into usable electrical energy via redox reactions occurring at the cathode and anode, where hydrogen peroxide (H_2O_2) is produced, Fe^{3+} is reduced to Fe^{2+}, and water is oxidized to oxygen, supporting continuous pollutant degradation reactions (Wang et al., 2021). To maintain the efficiency of the RED process, the decomposed NH_4HCO_3 is regenerated through a distillation process that recovers NH_4^+ and HCO_3^- components to produce fresh NH_4HCO_3, enabling a closed-loop operation. This continuous regeneration ensures sustained system performance, energy generation, and enhanced degradation of Persistent

Organic Pollutants (POPs) while producing environmentally benign byproducts such as oxygen and carbon dioxide (Tian & Wang, 2022).

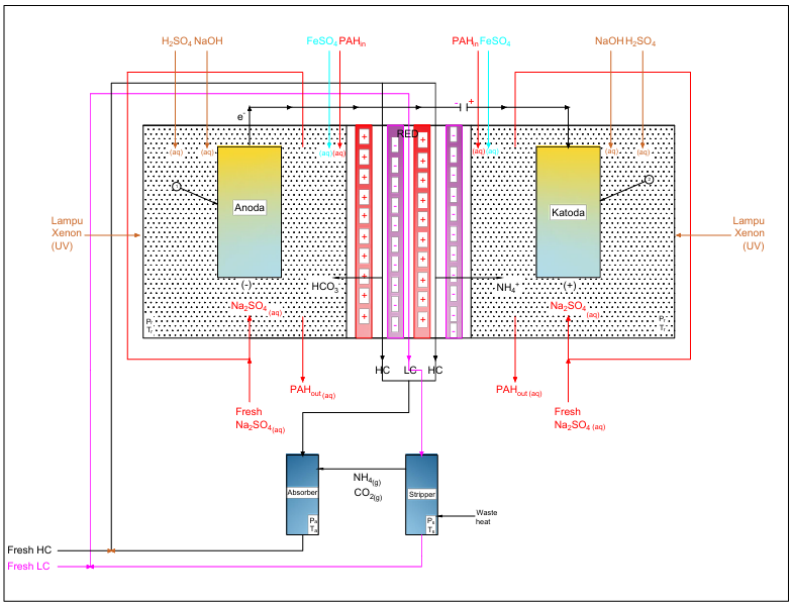

Fig. 1. Schematic diagram of PREC-Fenton

The interaction between the cathode and anode in the PREC-Fenton system plays a crucial role in maintaining the balance of pollutant degradation. At the cathode, H_2O_2 is generated to drive the Fenton reaction and Fe^{3+} ions are reduced to Fe^{2+}, while at the anode, water is oxidized to produce oxygen or directly oxidizes organic pollutants. This synergistic process supports continuous reactions and results in environmentally benign byproducts such as oxygen and carbon dioxide, thereby enhancing wastewater treatment efficiency (Tian & Wang, 2022; Wang et al., 2021). A detailed schematic of the reactions occurring in the PREC-Fenton system is presented in Table 1 below.

Table 1. Fenton reactions

Reactions	Reaction Equations	Description
Cathode Reactions	$O_2 + 2H^+ + 2e^- \rightarrow H_2O_2$	Electrochemical synthesis of H_2O_2 via two electron transfer (hydrogen peroxide electrosynthesis)
	$O_2 + 4H^+ + 4e^- \rightarrow 2H_2O$	Electrochemical synthesis of H_2O via four-electron transfer
	$2H_2O_2 \rightarrow 2H_2O + O_2$	Degradation of hydrogen peroxide (H_2O_2) into water and oxygen
	$H_2O_2 \rightarrow * HO_2 + H^+ + e^-$	Decomposition of H_2O_2 into peroxide radicals ($*HO_2$ and electrons)
	$* HO_2 \rightarrow O_2 + H^+ + e^-$	Decomposition of peroxide radicals ($*HO_2$) into oxygen (O_2), protons, and electrons
Anode Reactions	$2H_2O \rightarrow O_2 + 4H^+ + 4e^-$	Oxygen evolution reaction (oxidation of water into oxygen, protons, and electrons)
	$O_2 + 2H^+ + 2e^- \rightarrow H_2O_2$	Oxygen generated at the anode is utilized for H_2O_2 generation at the cathode through diffusion
	$R * H_2O \rightarrow CO_2 + H^+ + e^-$	Direct oxidation of organic pollutants (organic molecules oxidized into carbon dioxide, protons, and electrons)

(Deb et al., 2023; Smara et al., 2024)

To further optimize PREC-Fenton's operational performance in dynamic environments, the integration of Artificial Neural Networks (ANNs) with Proportional-Integral-Derivative

(PID) controllers offers a highly adaptive control solution (Getachew Gizaw et al., 2023). ANNs enable real-time adjustment of system parameters by learning operational patterns from process data, overcoming the limitations of traditional, static control systems (Leng et al., 2022). When combined with PID controllers that stabilize process variables, this ANN-PID hybrid ensures responsive, efficient, and reliable system operation even under fluctuating waste stream conditions. The application of this control architecture not only improves POP degradation performance but also enhances energy efficiency, positioning PREC-Fenton as an eco-intelligent, AI-driven water treatment technology capable of meeting both industrial wastewater management and environmental sustainability goals (Kasinathan et al., 2022).

The PREC-Fenton method has proven effective in degrading pollutants such as tetracycline, phenol, and ampicillin, with efficiencies exceeding 80% (Chen et al., 2020). The efficiency of the PREC-Fenton system depends on several factors, including H_2O_2 concentration, temperature, type of catalyst, and stirring speed. Optimizing these parameters enhances the generation of hydroxyl radicals necessary for the degradation of POPs. The PREC-Fenton system has been widely applied across various industrial sectors, including coal gasification. This technology has demonstrated high effectiveness, with reductions of COD by 92.4%, total phenols by 86.1%, and NH_4^+–N by 77.3% (Xu et al., 2019). Overall, PREC-Fenton offers an efficient, cost-effective, and sustainable solution for hazardous waste (B3) treatment. The photo-Fenton process at a semi-industrial scale exhibits a low environmental footprint, with greenhouse gas emissions ranging from approximately 2.71 to 0.762 kg CO_2eq per cubic meter of wastewater (Belalcázar-Saldarriaga et al., 2019; Foteinis et al., 2019), making it an environmentally friendly option for small and medium-sized industries.

The Thermolytic RED-Heat Engine (t-RED-HE) is then added to the system so that utilizes salinity gradients to generate electricity while simultaneously using low-grade waste heat to regenerate ammonium bicarbonate (NH_4HCO_3) solutions. This regeneration enables the solution to be reused in the Reverse Electrodialysis (RED) cycle, thereby improving the system's efficiency and sustainability (Tian & Wang, 2022). Unlike conventional RED systems that rely solely on salinity gradients, the t-RED-HE integrates thermal energy recovery from waste heat, making the system more energy-efficient and environmentally friendly (Leng et al., 2024). This technology offers a more efficient solution for sustainable applications such as PREC-Fenton, which combines pollutant degradation with electricity generation (Giacalone et al., 2020).

2. Methods

2.1 Research approach

This research employs a numerical simulation approach using Aspen Plus V11 and Simulink MATLAB R2024a to model the PREC-Fenton and t-RED-HE systems. The simulation is designed to optimize the degradation of persistent organic pollutants (POPs) through electrochemically controlled redox mechanisms. The objective of the modeling is to understand the dynamic interactions among system components, estimate key operational parameters, and identify potential energy savings and process efficiencies.

The initial data used in Aspen Plus and Simulink simulations are derived from calculations on three external components of the PREC-Fenton system, namely: t-RED-HE, the pumping system, and the regeneration unit. These calculations involve the configuration of critical variables such as electrochemical potential, electric current, and pump energy requirements. A detailed overview of the simulation approach is illustrated in Figure 2 below.

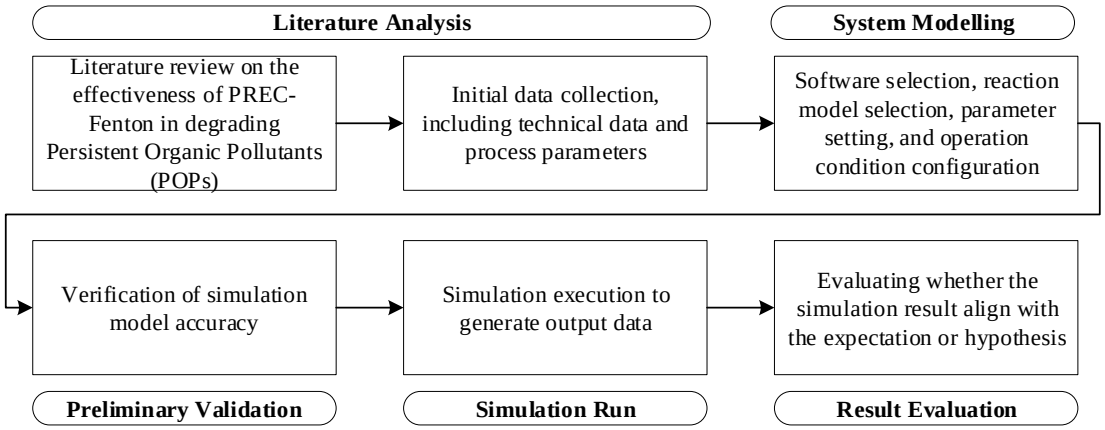

Fig. 2. Research approach

2.2 Research framework

This study employs an integrated multi-stage approach encompassing system design, simulation, and comprehensive analysis of results. The process begins with the steady-state design of the PREC-Fenton and t-RED-HE system models using Aspen Plus software, serving as the foundation for thermodynamic and process modeling. Once the base model is established, it is followed by electrochemical reaction simulations within the PREC-Fenton system to explore the reaction dynamics and mechanisms involved.

The next stage involves evaluating the degradation of Persistent Organic Pollutants (POPs) through Fenton redox reactions, which form the core of hazardous waste (B3) treatment in this system. To enhance system performance, optimization is conducted using an Artificial Neural Network (ANN) algorithm, including sensitivity analysis of various operational parameters such as pH, temperature, and reagent concentrations to determine the optimal configuration.

Additionally, this research includes an economic evaluation of the developed system, comprising calculations of Net Present Value (NPV), Internal Rate of Return (IRR), and Return on Investment (ROI) to assess its financial feasibility for implementation. For a more detailed overview of the research flow, refer to Figure 3, while the degradation rate determination presented in Figure 4 and design input flow in Aspen Plus are visually presented in Appendix 1.

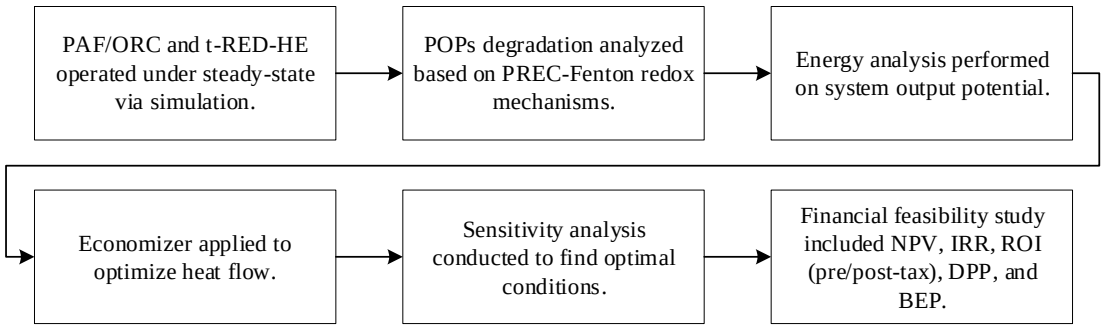

Fig. 3. Research framework

The Figure 4 illustrates the modeling process for the degradation of Persistent Organic Pollutants (POPs). It begins with establishing the basis for the degradation rate equation, followed by the modeling of POPs using specific parameters such as mass balance, concentrations (M, MX1, MX2), mass transfer coefficient (KLa), and stoichiometric coefficients. An ordinary differential equation (ODE) is then formulated to represent the degradation process of POPs. This ODE is solved using the Runge-Kutta method to derive a degradation rate equation. The results are simulated dynamically using Simulink to model

the system behavior over time, ultimately yielding insights into the dynamics of POP concentration reduction.

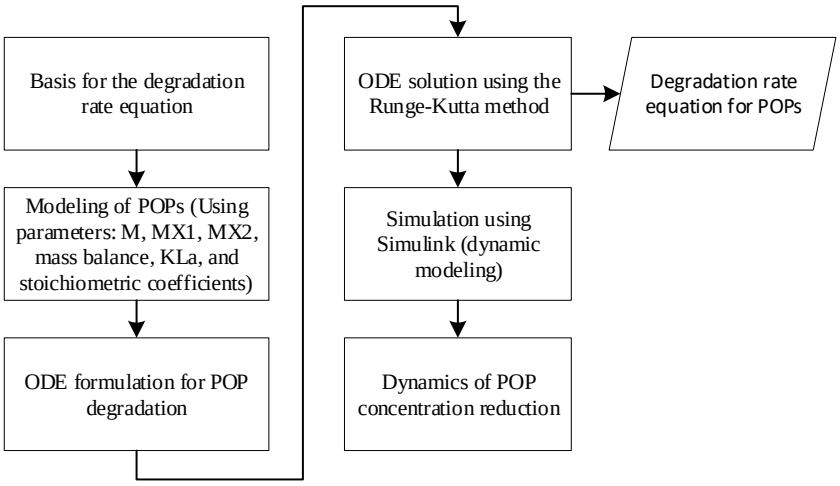

Fig. 4. Degradation rate determination scheme

2.3 System optimization method

The system optimization in this study aims to enhance energy efficiency in the PREC-Fenton system while ensuring operational stability through an Artificial Neural Network (ANN)-based approach. For a better understanding of the energy optimization workflow, refer to Figure 6 below.

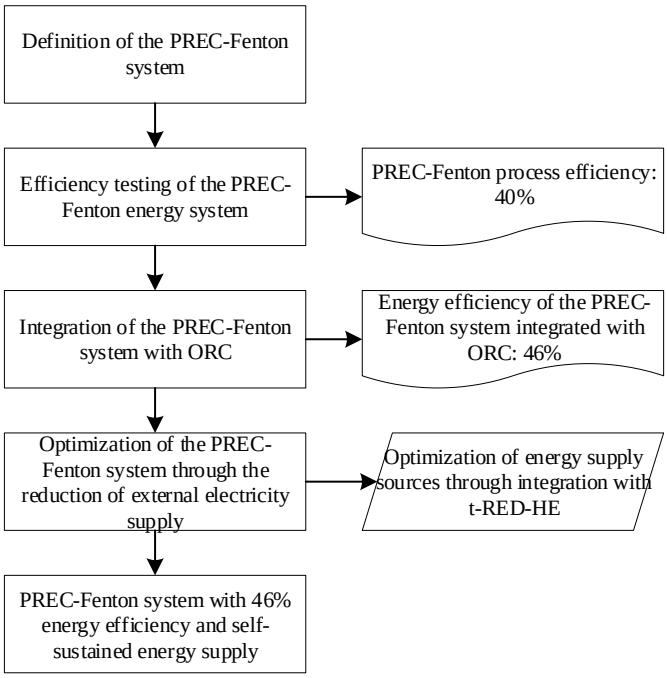

Fig. 6. Energy optimization scheme

The PREC-Fenton system requires adequate energy input to operate optimally. The integration of an Organic Rankine Cycle (ORC) as an internal component of the PREC-Fenton system enables optimized energy utilization, thereby improving the overall efficiency of the system. A visualization of the standalone PREC-Fenton system is presented in Figure 7, followed by the integrated PREC-Fenton and ORC configuration in Figure 8, and the standalone ORC system illustrated in Figure 9.

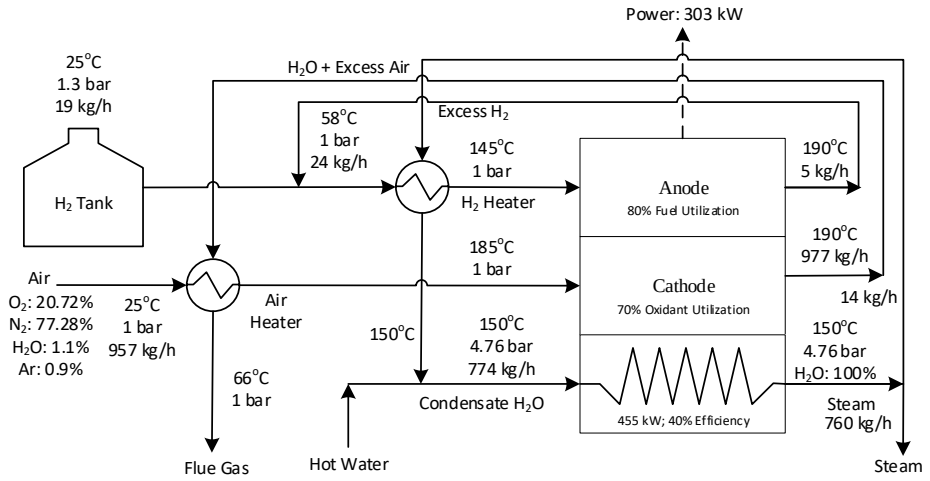

Fig. 7. System 1: Standalone PREC-Fenton baseline case
(Wilailak et al., 2021)

This process in Figure 7 illustrates the operation of a PREC-Fenton system for cogeneration, combining electricity and heat production. The system begins with ambient air (25 °C, 1 bar) and hydrogen from a storage tank (25 °C, 1.3 bar) as input. Air is preheated to 66 °C via an air heater before entering the cathode, while hydrogen is preheated in two stages—first to 58 °C and then to 145 °C—before entering the anode. Inside the PREC-Fenton, the anode operates at 190 °C with 80% fuel utilization, and the cathode at the same temperature with 77% oxidant utilization. The electrochemical reaction generates 303 kW of electric power and 455 kW of thermal energy, which is used to produce steam at 150 °C and 4.76 bar, with a flow of 760 kg/h. Additionally, hot water and small amounts of excess hydrogen (5 kg/h) and exhaust air (977 kg/h) are released (Wilailak et al., 2021). The system efficiently recovers waste heat for steam and water generation, making it ideal for combined heat and power (CHP) applications.

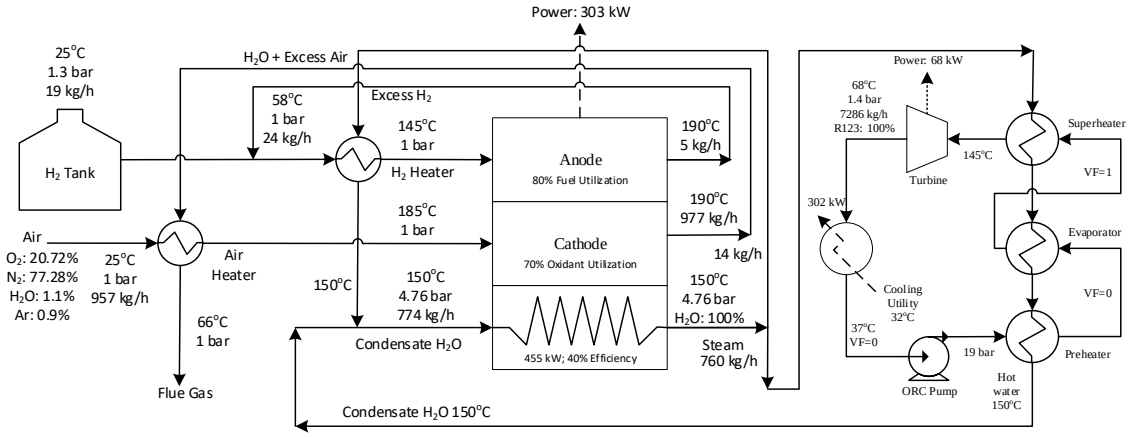

Fig. 8. System 2: Integration of PREC-Fenton system with ORC
(Wilailak et al., 2021)

This diagram presents a schematic of a PREC-Fenton system used for combined heat and power generation. The system utilizes hydrogen (H_2) from a storage tank and ambient air as reactants. The air is preheated to 66 °C using an air heater before entering the cathode. Hydrogen at 25 °C and 1.3 bar is first heated to 145 °C using a hydrogen heater and then delivered to the anode. Within the fuel cell, the anode operates at 190 °C with 80% fuel utilization, and the cathode at the same temperature with 77% oxidant utilization. The electrochemical reaction generates 303 kW of power, and heat released (455 kW) is used to

produce steam at 150 °C and 4.76 bar, with a flow rate of 760 kg/h. The system also delivers hot water and excess hydrogen and air as byproducts (Wilailak et al., 2021). This integrated PREC-Fenton setup efficiently generates electricity and heat, making it suitable for cogeneration applications.

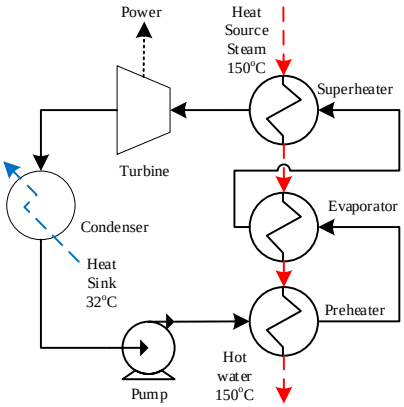

Fig. 9. ORC configuration

In addition to integration with the ORC, the PREC-Fenton system utilizes an external t-RED-HE module to enhance overall energy efficiency. The t-RED-HE technology is designed to harness salinity gradients and waste heat energy, generating additional power through an efficient electrodialysis process (Giacalone et al., 2020). The integration of the PREC-Fenton–ORC system with t-RED-HE not only reduces energy waste but also supports the operational sustainability of the system by ensuring optimal utilization of available thermal resources. A visualization of the t-RED-HE system is presented in Figure 10.

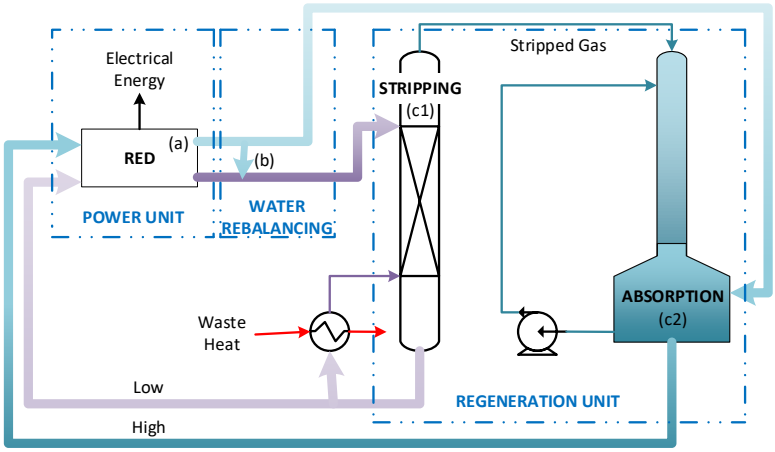

Fig. 10. Conceptual diagram of the t-RED-HE system. (a) power unit (RED unit), (b) Water balancing, (c1) stripping unit, and (c2) condensation/absorption unit

Optimization using an ANN-PID controller is employed to minimize prediction errors and enhance system stability during operation. The output of the ANN includes the optimal values of the PID control parameters—K_P, K_I, and K_D—as well as the system error, which is used to evaluate model performance based on metrics such as Root Mean Square Error (RMSE) and the coefficient of determination (R^2) (Smara et al., 2024). These metrics indicate the model's accuracy in predicting and regulating system parameters in real time (Bestwick et al., 2023; Seborg et al., 2020). The basic scheme of the ANN is illustrated in Figure 11.

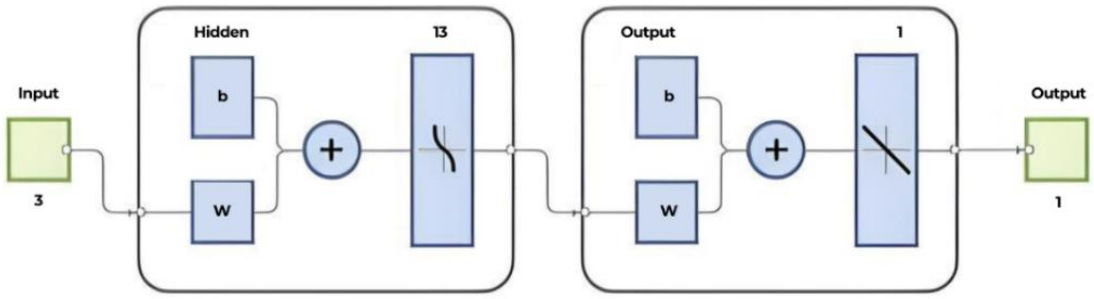

Fig. 11. Artificial neural network (ANN) diagram of the PREC-Fenton control system

2.4 Economic analysis determination

The economic evaluation includes key parameters such as Net Present Value (NPV), Internal Rate of Return (IRR), Discounted Payback Period (DPP), and Return on Investment (ROI) to assess the profitability and financial feasibility. The calculations for NPV, IRR, DPP, and ROI are based on the following formulas (Ranade et al., 2022):

$$NPV = \sum_{t=0}^{n} \frac{\pi t}{(1+i)^t} \quad \text{(Eq. 2)}$$

$$IRR = i_1 + \frac{NPV_1}{(NPV_1 - NPV_1)}(i_2 - i_1) \quad \text{(Eq. 3)}$$

$$DPP = A + \frac{B}{C} \quad \text{(Eq. 4)}$$

$$ROI = (\frac{Net\ Profit}{Investment\ Cost})\ x100\% \quad \text{(Eq. 5)}$$

The notation used in this analysis includes several key variables. The symbol πt represents the profit at time period *t*, where *t* indicates the specific time period under consideration. The variable *i* refers to the interest rate, expressed as a percentage. *A* denotes the last period in which the cumulative cash flow is negative, serving as a critical reference point for evaluating investment recovery. The variable *B* is defined as the absolute value of the cumulative net cash flow at the end of period *A*, highlighting the magnitude of the shortfall that needs to be recovered. Finally, *C* refers to the total cash inflow received during the period(s) subsequent to period *A*, which is essential in assessing the subsequent financial recovery or gain after the negative cash flow phase.

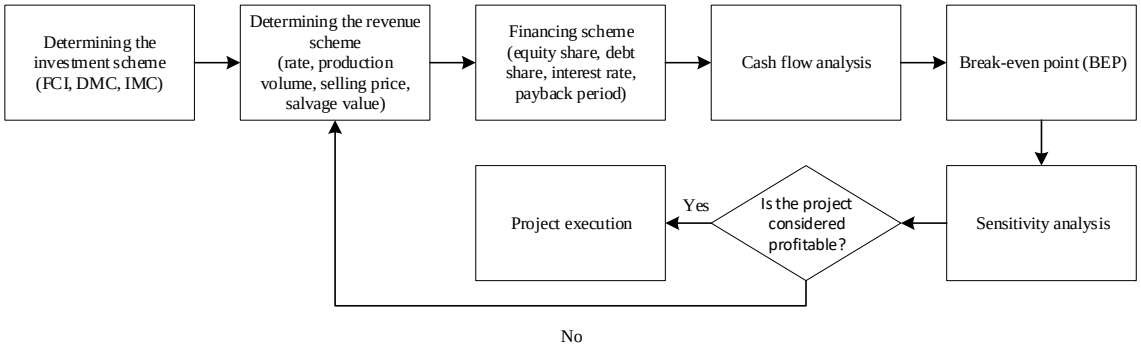

Fig. 12. Schematic diagram of economic feasibility analysis determination

In this simulation, the calculation of capital expenditure (CAPEX), operational expenditure (OPEX), and annual revenue projections serve as the basis for obtaining a comprehensive understanding of the system's financial feasibility. The economic simulation

is carried out by referring to the energy production data and the degradation rates of persistent organic pollutants (POPs) obtained from previous technical simulations. For further insights into the flow and results of the economic analysis, readers are referred to Figure 12 above, which provides a detailed visualization of the financial assessment.

3. Results and Discussion

3.1 Degradation of persistent organic pollutants

3.1.1 System flowsheet

There are three main components in the overall system: PREC-Fenton, STACK PREC-Fenton, and t-RED-HE. PREC-Fenton is a technology that integrates the Fenton reaction with Reverse Electrodialysis (RED), while the STACK PREC-Fenton serves as the core unit where the degradation reaction occurs using H_2O_2 and Fe^{2+} as catalysts. Meanwhile, t-RED-HE is an independent RED-based power generation system designed to sustainably support the operation of the PREC-Fenton process.

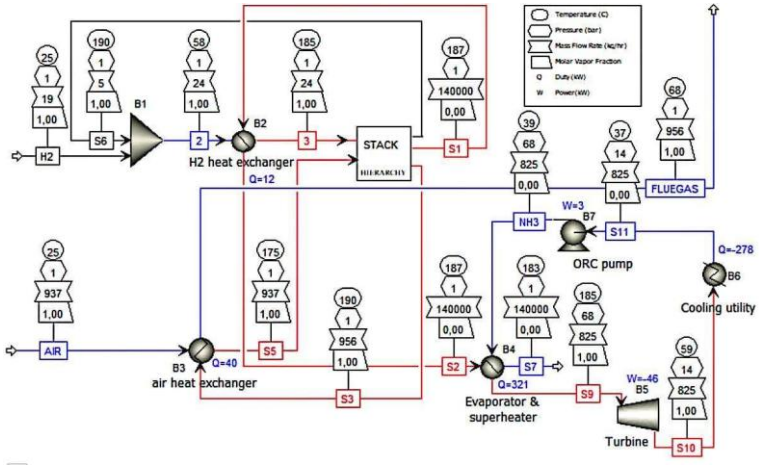

Fig. 13. Flowsheet unit PREC-Fenton

The Figure 14 illustrates a combined heat and power (CHP) system based on a fuel cell integrated with a thermal oil loop. Hydrogen and air are supplied at specified conditions and enter the fuel cell unit (B1), where electrochemical reactions produce both electricity and heat. The anode and cathode outlets exit through B2, with the anode stream showing no heat recovery, while the cathode stream passes through a heat exchanger (B9). Here, thermal oil absorbs 300 kW of heat, increasing in temperature from 183 °C to 187 °C. This recovered thermal energy is then distributed for power generation (333 kW) and heating (300 kW), demonstrating an efficient utilization of both electrical and thermal outputs in the system.

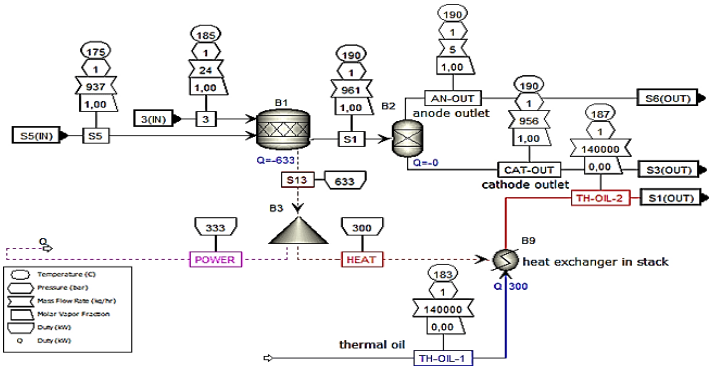

Fig. 14. Flowsheet STACK PREC-Fenton

The flowsheet includes the main equipment used in the PREC-Fenton system. It illustrates the overall process flow, including the pathways of H_2O_2 and Fe^{2+} reactants, as well as the output streams of products and waste. Key components such as connecting pipelines and flow control mechanisms are also shown to provide a detailed view of the system. Further details are presented in Figure 13 for the PREC-Fenton Flowsheet, Figure 14 for the STACK PREC-Fenton Flowsheet, and Figure 15 for the t-RED-HE Flowsheet.

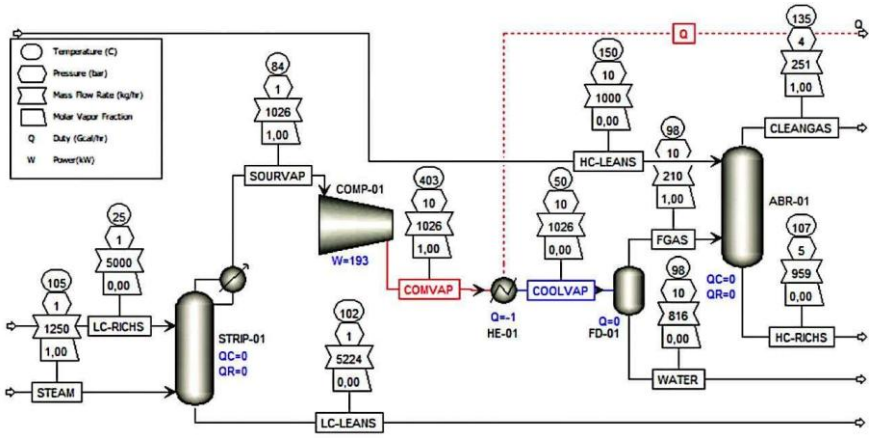

Fig. 15. Flowsheet t-RED-HE

3.1.2 System modeling results

This modeling aims to estimate hydrogen production and the required membrane area. Hydrogen production in this system is considered a secondary product. The initial data from Tables 2 to 6 were used to define the PREC-Fenton system (Kwon et al., 2015; Raka et al., 2020; Tarascon, J. M., & Simon, P., 2015). The modeling results indicate an electro-Fenton potential of 2.13 V with 30 unit cells. The hydrogen production rate reaches 0.83 mol $H_2/m^2 \cdot h$, with a total current of 195.46 A, requiring a membrane area of 123.45 m^2. The pumping power is 0.00035 W/m^2, and the regeneration heat demand is 0.054 kW. This design serves as the basis for input variables in the Aspen Plus simulation.

Table 2. Technical and economic input data for the PREC-Fenton model

Parameters	Symbol	Value	Unit
Equivalent molar conductivity	Λ_0	90	
Model parameter 1	A_Λ	41.55	
Model parameter 1	B_Λ	0.6023	
Model parameter 1	C_Λ	0	
Activity coefficient 1	g_1	0.13661	I/mol
Activity coefficient 1	g_2	1.0007	I/mol
Ideal gas constant	R	8,314	J/(mol.K)
Temperature	T	293	K
Concentrate solution concentration	C_{hc}	2	M
Dilute solution concentration	C_{ic}	0.06	M
Faraday's constant	F	96,485	C/mol
Permselectivity of CEM/AEM	$\alpha_{cem}=\alpha_{aem}$	0.753	
Fitting parameter	r_1	0.0002	$\Omega m^2/m$
Inter-membrane distance	$\delta_{ic}=\delta_{hc}=\delta_{ch}$	270	μm
Porosity	ε	0.8	
Anode voltage	$E_{an}(Fe^{2+}\rightarrow Fe^{3+})$	0.77	V
Cathode voltage	E_{cat} $(O_2\rightarrow H_2O_2)$	0.68	V
Activation factor	α	0.5	
Current (instantaneous)	i	10	A/m^2
Exchange current	i_0	0.01	A/m^3
Number of electrons transferred in the reaction	$Z_{an}=Z_{cat}$	2	e^- transferred in the reaction

Cell resistance	R_{cell}	1	Ω
Cell current	I_{cell}	0.1	A
Electrode resistance	R_{ele}	0.01	Ωm^2
Valence ions per mole of H_2	z	2	Z = 2 valence ions per mole of H_2
Valence ions per mole of POP	z	1	Valence ions per mole of POP
Losses	losses	0.06	
Faradaic efficiency	n_F=10%-losses	0.94	
POP reaction rate	r_{POP}	1x10-06	Mol/s
Treated wastewater concentration	$m_{TW\ Cap}$	0.476	Kg/s
Reaction conversion	Konversi	0.990	
Wastewater capacity	$M_{WW\ Cap}$	0.480	Kg/s
POP content	%POP	0.001	
POP capacity	$m_{POP\ Cap}$	0.00048	Kg/s
Molecular weight of POP	mw_{POP}	252,310	g/mol
Number of membrane pairs	N	10	
Dilute solution flow rate	V_{Ic}	0.01	m/s
Channel width	w	0.1	m
Water viscosity	μ	0.0009	Pa.s
Channel length	I	0.1	m
Water density	ρw	0.997	Kg/l
Density change per mass	$\frac{\Delta\rho}{\Delta m}$	0.0324	$Kg^2/(mol.l)$
Diffusivity coefficient (MEM)	D_{AmB}	$2x10^{-12}$	m^2/s
Membrane thickness	δ_{mem}	125	μm
Input concentration	C_1	0.08	M
RED stack	$C_{mem}=C_{RED\ stack}$	150	$\$/m^2$
Regeneration system cost	C_{regen}	3400	$\$/m^3/h$
Pump system cost	C_{pump}	300	\$/kW
Infrastructure cost	C_{infra}	1123	$\$/m^2$
Discount factor	r	0.06	
Plant life time	t	20	Years
Waste heat price	C_{heat}	0.01	\$/kWh
Operating hours per year	T_0	8,000	h
Hydrogen price	C_{H2}	3.59	\$/kg

The Table 3 (Raka et al., 2020) presents the input parameters used for scenario analysis of the PREC-Fenton system, comparing current, market, and future values. The concentration of the hydroxyl complex (C_{hc}) is currently 2 M, with both market and future values projected at 2.6 M. The concentration of the ligand complex (C_{lc}) starts at 0.06 M, with market and future estimations at 0.05 M and 0.07 M, respectively. The membrane transport coefficient ($\alpha_{cem} = \alpha_{aem}$) improves from 0.753 to 0.85 (market) and 0.95 (future), measured in Ωm^2/M μm. The reaction rate constant (r_1) is 0.0002 s^{-1} initially, with market and future values declining to 0.00004 s/year. Channel thickness (δ_{ch}) is 270 μm currently and is expected to reduce to 100 μm in both market and future cases. The Faradaic efficiency (n_F) is 0.94 at present, rising slightly to 0.95 (market) and 0.99 (future). Residence time (t_{res}) drops from 70 s to 60 s (market) and 50 s (future), while membrane lifetime (t_{mem}) increases from 4 to 7 and 10 years, respectively. These parameter shifts highlight efforts to enhance system efficiency, durability, and performance in the PREC-Fenton process.

Table 3. Input parameters of the PREC-Fenton system for scenario study

Parameters	Current Value (p)	Market Value (m)	Future Value (f)	Unit
C_{hc}	2	2.6	2.6	M
C_{lc}	0.06	0.05	0.07	M
$\alpha_{cem} = \alpha_{aem}$	0.753	0.85	0.95	-

r_1	0.0002	0.00004	0.00004	s^{-1}
δ_{ch}	270	100	100	µm
n_F	0.94	0.95	0.99	-
t_{res}	70	60	50	s
t_{mem}	4	7	10	year

The AmB-RED system model evaluates key parameters under current, market, and future scenarios to assess performance improvements. Conductivity and activity coefficients vary with concentration, affecting electrochemical behavior. The unit cell's open circuit voltage rises from 0.14 V to 0.19 V, while membrane and channel resistances significantly decrease, lowering total unit cell resistance. This boosts current density from 47.42 to 246.60 A/m^2 and raises hydrogen production from 0.83 to 4.32 mol H_2/m^2·h. The number of unit cells required drops from 30 to 23, and the membrane area is reduced from 123.45 m^2 to 17.09 m^2, indicating improved system efficiency and compactness.

Table 4. t-RED modeling

Modeling of the AmB-RED System					
1. Solution Conductivity The equivalent conductivity of ammonium bicarbonate depends on its concentration and the molar conductance, which is temperature-dependent. Here A, B, C are model parameters used for fitting and referred from Bevacqua et al., (2017). The conductivity is calculated at a constant temperature of 293 K using the Jones-Dole equation. $\Lambda = \Lambda_0 - \frac{A_\Lambda \Lambda_i . C_i^{1/2}}{1 + B_\Lambda . C_i^{1/2}} - C_\Lambda C_i$ $k\ (mS/cm) = \Lambda . C_i$		Current Value (p)	Market Value (m)	Future Value (f)	
	hc	58.27	56.01	56.01	
	lc	81.13	81.81	80.52	
	hc	116.54	145.63	145.63 mS/cm	
	lc	4.87	4.09	5.64 mS/cm	
2. Activity Coefficient of the Solution The activity coefficient depends on the molar concentration of the salt (Bevacqua et al., 2017). The linear dependence of the activity coefficient on concentration is estimated using the ENTRL-RK thermodynamic package in Aspen Plus. $\gamma = g_1 . C_i + g_2$	hc	1.27	1.36	1.36	
	lc	1.01	1.01	1.01	
3. Unit Cell Open Circuit Potential The membrane potential (V) for a pair of cells (CEM, AEM) without considering any losses. The electrochemical potential difference across an Ion Exchange Membrane (IEM) placed between two solutions of different concentrations can be calculated using a modified Nernst equation. $E_{u.c}^{ocp}\ (V) = (\alpha_{cem} + \alpha_{aem}) . \frac{R.T}{F} . ln\left(\frac{\gamma_{hc} C_{hc}}{\gamma_{lc} C_{lc}}\right)$	0.14	0.18	0.19	V	
4. Area Specific Membrane Resistance The ohmic resistance of the membrane when immersed in solution, expressed as a function of ion concentration in the solution. $R_{cem}(\Omega m^2) = R_{aem} = r_1 . (C_{lc})^{-0.236}$	0.0004	0.0001	0.0001	Ωm^2	
5. Channel Ohmic Resistance Resistance caused by the solution in the geometry of the channel and spacer. This resistance depends on concentration and is calculated using the molar conductivity of the salt. $R_{lc}\ (\Omega m^2) = \frac{\delta_{lc}}{\varepsilon k_{lc} C_{lc}}$	0.0007	0.0003	0.0002	Ωm^2	
$R_{hc}\ (\Omega m^2) = \frac{\delta_{hc}}{\varepsilon k_{hc} C_{hc}}$	0.0000290	0.0000086	0.0000086		
6. Unit Cell Resistance The total cumulative resistance of the membrane and the channel within a single unit cell.					

	$R_{u.c}(\Omega m^2) = R_{cem} + R_{aem} + R_{lc} + R_{hc}$	0.0015	0.0005	0.0004	Ωm²
7.	Current Density at Peak Power The current density at peak power occurs when the operating potential is half of the open circuit voltage. Assuming constant resistance, the current density [A/m²] at peak power is calculated using Ohm's law. $j_{u.c}^{pp}(A/m^2) = \frac{E_{u.c}^{ocp}}{2.R_{cell}}$	47.42	191.37	246.60	A/m²
8.	Actual Unit Cell Potential The actual potential across the RED unit cell decreases due to ohmic resistance within the unit. $E_{u.c}^{act}(V) = E_{u.c}^{ocp} - R_{u.c}.j_{u.c}^{pp}$	0.07	0.09	0,09	V
9.	Required Potential for Photoelectro-Fenton $\eta_{an} = \eta_{cat} = \frac{R.T}{\alpha.z.F} ln\left(\frac{i}{i_0}\right)$	0.17	0.17	0.17	V
	$\boldsymbol{E_{fef} = E_{an} + E_{cat} + \eta_{an} + \eta_{cat} + I_{cell}.R_{cell}}$	2.13	2.13	2.13	V
10.	Number of Unit Cells The minimum number of unit cells required to be connected in series. $\boldsymbol{N_{u.c}(Unit\ cell) = \frac{E_{fef}}{E_{u.c}^{act}}}$	30	23	23	unit cell
11.	Stack Open Circuit Potential The open circuit potential of the RED stack (V), which drops when the RED device is connected to an external load $\boldsymbol{E_{stack}^{act}(V) = N_{u.c}.E_{u.c}^{act}}$	2.13	2.13	2.13	V
12.	Total Stack Resistance The total resistance in the stack, which includes the sum of all unit cell resistances and electrode resistance. $R_{stack}(\Omega m^2) = N_{u.c}.R_{u.c} + R_{ele}$	0.05	0.02	0.02	Ωm²
13.	Hydrogen Production Rate The theoretical amount of hydrogen (in moles) produced per unit time in the electrode-electrolyte washing compartment of the RED stack. $\boldsymbol{\dot{n}\ H_2 = \frac{j_{u.c}^{pp}.3600}{z.F}\eta_F}$	0.83	3.36	4.32	Mol $H_2/m^2.h$
14.	Total Stack Current in Parallel $\boldsymbol{I_{para}^{pp} = \frac{m_{POP}^{cap}.1000.z.F}{mw_{POP}.\eta_F}}$	195.46	193.40	185.58	A
15.	Membrane Area $\boldsymbol{A_{mem}^{tot} = \frac{I_{para}^{pp}.N_{u.c}}{j_{u.c}^{pp}}}$	123.45	23.61	17.09	m^2

The pump system (Table 5) modeling focuses on fluid dynamics within the RED unit. The low-concentration (LC) solution flow rate remains constant at 0.0000022 m^3/s across all scenarios, while the hydraulic diameter slightly decreases from 0.000402 m to 0.000395 m due to tighter spacer packing. This leads to increased pressure drops (38.24 to 55.51 Pa) and higher pumping power requirements (0.00035 to 0.00070 W/m^2). The Reynolds number remains stable, indicating laminar flow conditions. In mass balance modeling, salt flux increases with concentration difference, from 5×10^{-4} to 3×10^{-3} $mol/s\cdot m^2$. The regeneration system modeling shows heat demand for ammonium bicarbonate removal ranging from 6.99 to 5.51 kWh/m^3, with associated power dropping from 0.066 to 0.043 kW, reflecting improved thermal efficiency in future scenarios.

Table 5. Pump system modeling, mass balance, and t-RED regeneration system

Pump System Modeling	
1	Flow Rate The velocity of the low-concentration (LC) solution affects the double-layer resistance and, consequently, the power density. The flow rate m^3/s for the low-concentration feed solution is estimated using the following equation:

$Q_{lc}(m^3/s) = N.v_{lc}.\delta_{ch}.w.\varepsilon$	0.0000022	0.0000022	0.0000022		
2. Hydraulic Diameter Spacer filaments obstruct the flow through the channel, requiring additional pumping power. To estimate the influence of spacer filaments, the hydraulic diameter of the spacer-filled channel can be calculated using the following equation:					
$d_{h,lc}(m) = d_{h,hc} = \frac{4\varepsilon}{\frac{2}{\delta_{ch}} + \left((1-\varepsilon).\frac{\alpha}{\delta_{ch}}\right)}$	0.000402	0.000398	0.000395	m	
3. Pressure Drop In the ideal case of fully developed laminar flow, the pressure drop (Pa) can be estimated using the Darcy-Weisbach equation as follows:					
$\Delta p_{lc}(Pa) = \Delta p_{hc} = \frac{12.\mu.l^2}{0{,}25.d_h^2.t_{res}}$	38.24	45.42	55.51	Pa	
4. Pumping Power The power [W/m^2] required to overcome hydraulic resistance while pumping the feed solution through the channels strongly depends on the spacer porosity, as this determines the hydraulic radius that affects pressure drop. The required power can be calculated using the following equation:					
$P_{pump}(W/m^2) = \frac{\Delta p_{lc}.d_{h,lc}.\varepsilon}{t_{res}} + \frac{\Delta p_{hc}.d_{h,hc}.\varepsilon}{t_{res}}$	0.00035	0.00048	0.00070		
5. Reynolds Number The Reynolds number (Re) for a wide channel corrected by spacer porosity is defined as the ratio of inertial forces to viscous forces in the fluid. For spacer-filled channels, the Reynolds number corrected by spacer porosity can be expressed as:					
$\rho\ (kg/l) = \rho_w + \left(\frac{\Delta\rho}{\Delta m}\right)m$	0.9989	0.9986	0.9993	kg/l	
$Re = \frac{\rho.v_{lc}.d_h}{\mu}$	0.00446	0.00442	0.00438		
Mass Balance Modeling					
1. Salt Flux The concentration difference between adjacent channels drives the salt flux from the high-concentration channel to the low-concentration channel.					
$J_{salt} = \frac{j^{pp}}{F} + 2.\frac{D_{AmB}.(C_{hc}^{in} - C_{lc}^{in})}{\delta_{mem}}$	5x10^{-04}	2x10^{-03}	3x10^{-03}	mol salt/s.m^2	
Regeneration System Modeling					
1. Regeneration Heat Demand The total thermal power required to remove ammonium bicarbonate (NH_4HCO_3) salt from the low-concentration (LC) solution:					
$\dot{q}_{th}(kWh/m^3) = a_1 e^{a_2 C_1} - a_3 C_2^{a_4} + a_5 C_1^{a_6} C_2^{a_7}$	6.99	8.49	5.51	kWh/m^3	
$q_{regen}(kW) = \dot{q}_{th}.Q_{lc}.3600$	0.054	0.066	0.043	kW	

Table 6, retrieved from Bevacqua et al. (2017), presents the equation parameters (a_1 to a_7) used to model the behavior of the solution entering the stripper column as a function of its concentration (C_1). These parameters vary across four defined concentration intervals: $0.025 \le C_1 \le 0.1$, $0.1 < C_1 \le 0.2$, $0.2 < C_1 \le 0.56$, and $0.56 < C_1 \le 2$. Each range corresponds to a unique set of coefficients, indicating how the model adjusts to changes in input concentration. Notably, parameter values for a_3 and a_5 significantly decrease as the concentration increases, reflecting reduced values in high-concentration scenarios, which likely influence mass transfer or energy consumption characteristics in the stripper process.

Table 6. Equation parameters as a function of the concentration of solution entering the stripper column

Concentration Range	a_1	a_2	a_3	a_4	a_5	a_6	a_7
0,025=<C_1=0,1	12.115	0.260	261.787	0.615	297.460	0.252	0.478

0,1<C_1<=0,2	12.836	1.020	258.324	0.612	260.000	0.165	0.517
0,2<C_1<=0,56	13.195	0.686	60.592	0.667	55.934	0.687	0.212
0,56<C_1<=2	8.714	0.225	35.796	0.656	45.560	0.758	0.045

3.1.3 PREC-fenton reaction modeling results

The modeling results of the PREC-Fenton reaction provide mass balances for each system, namely the PREC-Fenton system, the STACK PREC-Fenton system, and the t-RED-HE system. These mass balances represent the initial outcomes of the modeling process and serve as a foundation for further analysis. The simulation shows that H_2O_2 was input at a constant flow rate of 0.14318 mL·min^{-1}, with a total volume of 8.5909 mL (271.29 mmol) over a 3-hour period. Activation was carried out during the intervals of 0–15 minutes and 30–75 minutes. The simulation results also illustrate output profiles including concentrations of POP, H_2O_2, and O_2, directly reflecting the process efficiency. Furthermore, the reaction dynamics are demonstrated through the transformation of organic species (M, MX1, MX2), radicals (R), and iron species (Fe^{2+}, Fe^{3+}). The transformations involve a stepwise conversion from M to MX1 and MX2, ultimately leading to an asymptotic decrease in POP concentration. The normalized concentration profiles indicate the interrelation between H_2O_2 concentration, iron species, and radicals (R), as well as the presence of unproductive H_2O_2 decomposition. The reaction modeling profiles of the PREC-Fenton system are shown in Figure 16.

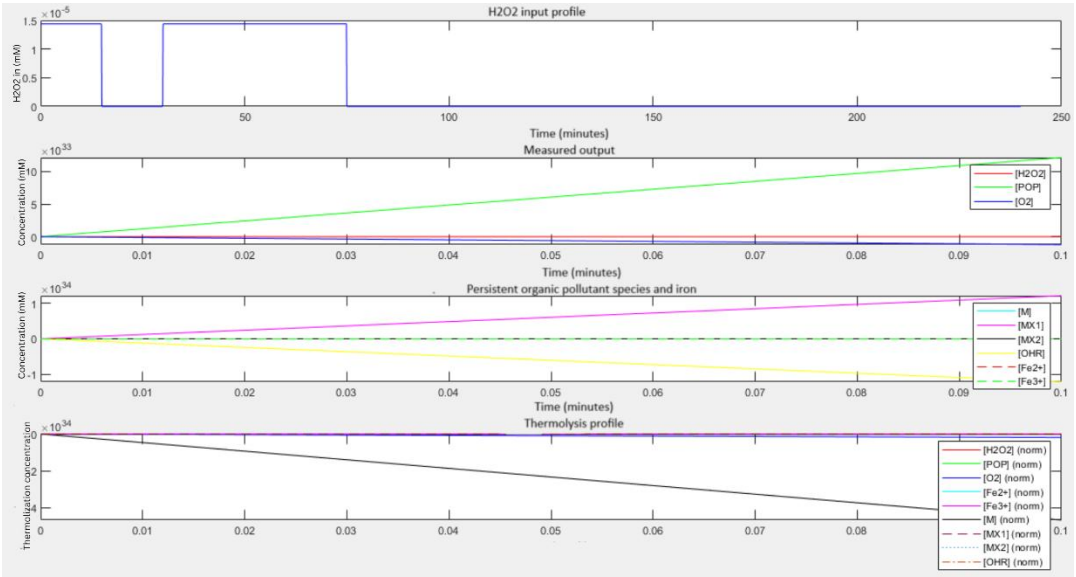

Fig. 16. Profile of POP degradation parameters over time: (a) H_2O_2 input, (b) Measured output of H_2O_2, POP, and O_2, (c) Species of persistent organic pollutants M, MX1, MX2, OHR, Fe^{2+}, Fe^{3+}, and iron, (d) Normalized profiles

3.1.4 Degradation efficiency

The simulation results indicate that the PREC-Fenton system is capable of degrading Persistent Organic Pollutants (POPs) with an efficiency of up to 99.99%, equivalent to 1,038.8 kg/hour of pollutants successfully decomposed into harmless compounds. This outcome represents a significant improvement compared to conventional technologies such as coagulation-flocculation, which typically achieve only around 30% efficiency. This achievement makes the PREC-Fenton system highly relevant for industries requiring complex wastewater treatment solutions. In addition, the PREC-Fenton system is able to produce 176.24 kg/hour of clean water along with carbon dioxide as a by-product. This high efficiency is achieved through the optimization of key operational parameters such as H_2O_2 concentration, catalyst type, temperature, and stirring speed, all of which enhance the

formation of hydroxyl radicals as the primary agents of degradation. Detailed information on the reaction mechanisms can be found in Table 1: Fenton Reactions.

3.2 System optimization

3.2.1 System integration with ORC

Based on the simulation and mass balance analysis, the PREC-Fenton system demonstrates an energy conversion efficiency of 40%. This efficiency was successfully increased to 46.13% through the integration of an Organic Rankine Cycle (ORC), contributing an additional 6.13%. The ORC utilizes waste heat to drive a working fluid through a turbine, thereby enhancing the overall system performance. These results indicate that the ORC integration not only boosts electricity generation but also reduces thermal emissions to the environment, thus supporting the overall sustainability of the process. Furthermore, this integration enables additional electricity production of up to 300.17 kW. The system integration flowsheet with ORC can be seen in Figure 8.

3.2.2 Integration with t-RED-HE

The PREC-Fenton system is also integrated with a Thermolytic Reverse Electrodialysis Heat Engine (t-RED-HE) to further enhance the efficiency of wastewater treatment and energy production. The t-RED-HE technology utilizes salinity gradients and waste heat energy to generate additional electricity through the electrodialysis process. Integration with t-RED-HE enables the recovery and utilization of residual thermal energy from the Organic Rankine Cycle (ORC), thereby reducing energy waste and eliminating the need for external energy input for the PREC-Fenton system.

3.2.3 Sensitivity analysis

The sensitivity analysis in this study aims to evaluate the impact of various operational parameters on the performance of the t-RED-HE system, with a focus on process efficiency and operational cost reduction. The first parameter analyzed is the steam mass flow rate, where an increase in steam flow was found to significantly affect the system's pH. This pH reduction is attributed to the increased concentration of H^+ ions generated from hydrolysis reactions, which can destabilize the system and thus require operational adjustments to maintain reaction equilibrium. The effect of steam mass flow rate on pH is illustrated in Figure 17 below.

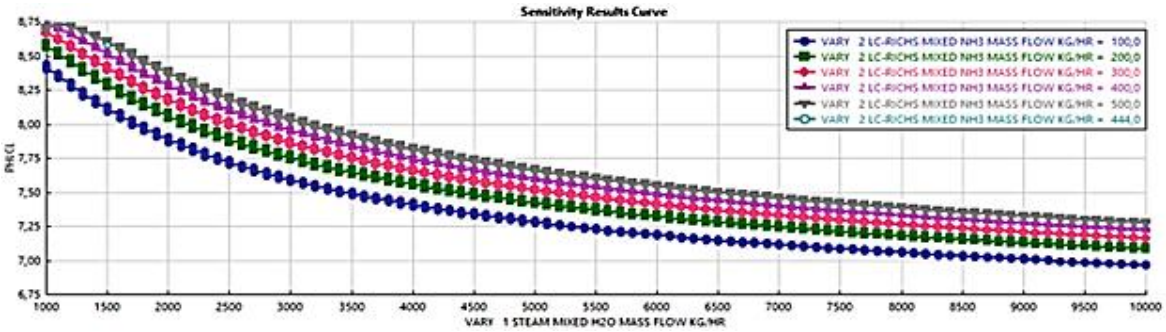

Fig 17. Sensitivity analysis graph of steam mass flow rate and NH_3 concentration on the pH of the low concentration lean stream in the t-RED unit

Next, operating pressure also shows a significant influence on the system. An increase in pressure enhances NH_3 solubility in accordance with Henry's Law, which increases the mass fraction of NH_3 and accelerates the dissolution of both NH_3 and CO_2 derived from the

decomposition of NH_4HCO_3. This positive effect contributes to higher regeneration flow concentrations, reducing the demand for fresh raw materials and directly lowering operational costs, as visualized in Figure 18.

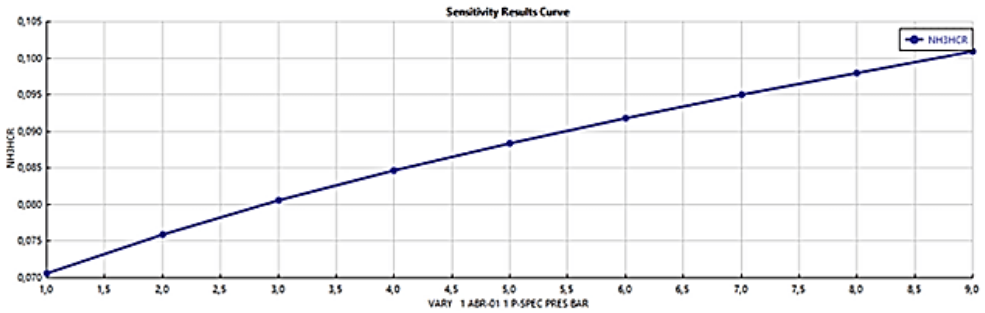

Fig 18. Sensitivity analysis graph of stage 1 pressure at ABS-01 on the NH_3 mass fraction in the high concentration RICHS (HC RICHS) stream

The third parameter is temperature, which, although capable of accelerating reaction rates, also poses risks to overall system efficiency. Uncontrolled temperature increases may reduce the NH_3 mass fraction due to evaporation, ultimately decreasing the overall efficiency of the process if not offset by adjustments in other parameters. The effect of temperature on system performance is shown in Figure 19.

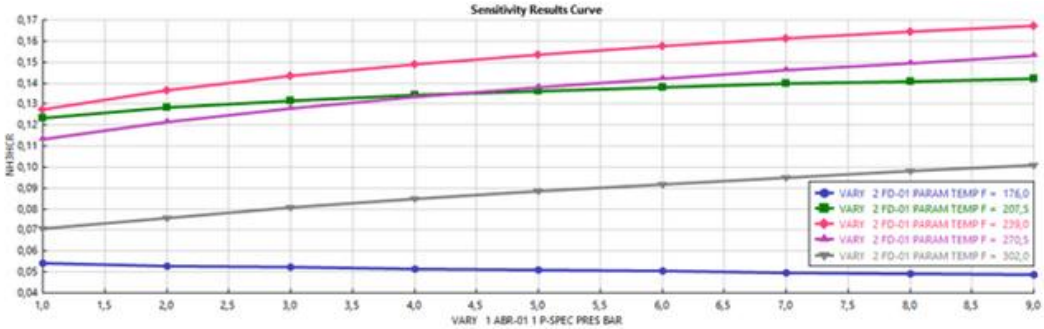

Fig 19. Sensitivity analysis graph of FD-01 temperature within the flash temperature range

Through this sensitivity analysis, the system is optimized by precisely controlling steam flow rate, pressure, and temperature to maintain the NH_4HCO_3 concentration equivalent to the initial input. This strategy enables effective regeneration and recirculation of materials without the need for continuous raw material replenishment, thereby enhancing process efficiency and significantly reducing operational costs.

3.2.4 System optimization through PID controller and ANN integration

Further optimization was conducted using an Artificial Neural Network (ANN) as a fitting tool for the PID controller parameters of the PREC-Fenton system. The results demonstrated excellent performance in predicting and optimizing the system parameters. The ANN model used in this study has three input variables, namely the K_P, K_I, and K_D parameters of the PID controller, with 13 neurons in the hidden layer and one neuron in the output layer. The optimal number of neurons was determined by analyzing the relationship between the number of neurons and the RMSE on both the training and validation sets. For further illustration, Figures 20–24 below provide a graphical visualization of the neuron-RMSE relationship analysis.

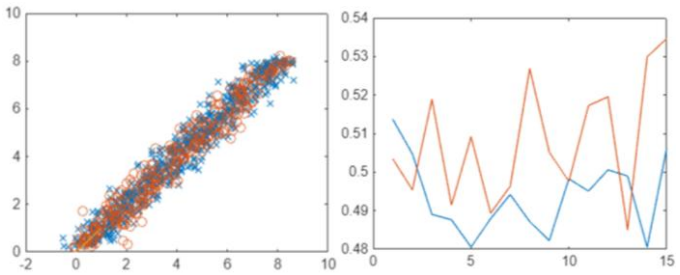

(a) (b)

Fig. 20. Graphs of (a) yTrainTrue (symbol x) versus yValTrue (symbol o), and (b) the number of neurons in the hidden layer (horizontal axis) versus RMSE of the training set (blue line) and validation set (orange line).

Based on the graph, it was found that the configuration of 13 neurons in a single hidden layer produced the lowest RMSE, with values of 0.4838 for the training set and 0.5160 for the validation set, corresponding to a deviation of approximately 5% within the output data range of 0 to 10. The ANN prediction results shown in Figure 21 demonstrate very high accuracy, with R^2 values for the K_P, K_I, and K_D parameters—relative to the output error of the PREC-Fenton control system—of 0.96594, 0.96529, and 0.96753, respectively. These values indicate a strong linear relationship between the predicted and actual results.

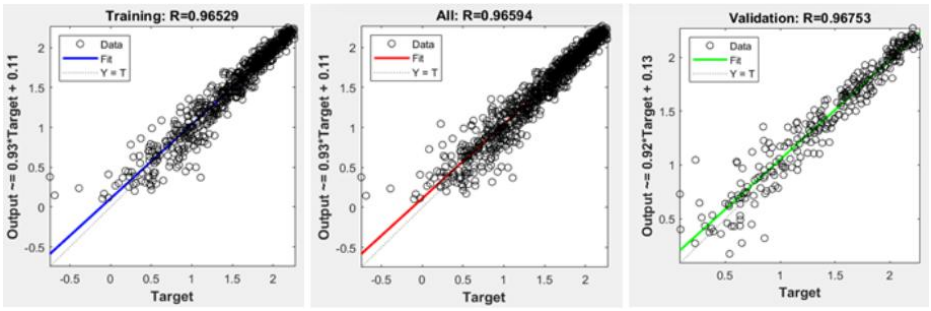

Fig 21. Regression graph of input variables K_I (blue), K_D (green), K_P (red) vs. output variable error

In addition, the model's best performance was achieved at the 18th epoch, with a minimum RMSE value of 0.0173, demonstrating the ANN's strong capability in significantly minimizing error. Figures 22, 23, and 24 below provide a visual representation of the simulated error behavior. These results indicate that the combination of ANN and PID controller is capable of producing a lightweight and efficient predictive model with a very low error rate.

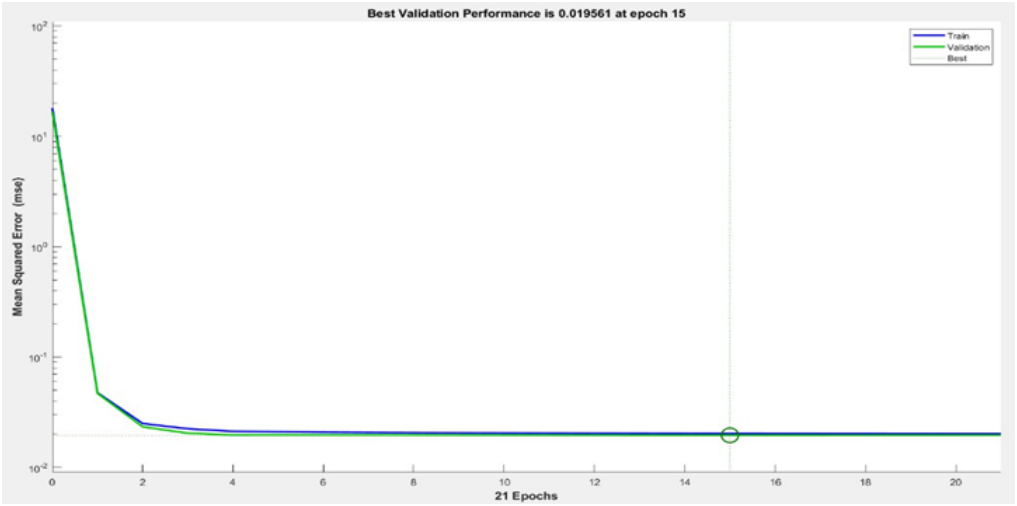

Fig. 22. Training plot: Performance

Figure 23 displays the error distribution (error = target − output) of a neural network model using 20 bins. Blue bars represent training data, green bars represent validation data, and the orange line indicates zero error. Most errors are concentrated around zero, particularly between -0.025 and 0.025, suggesting high prediction accuracy with minimal deviation. The symmetric shape and absence of extreme outliers indicate good model performance, stable generalization, and no signs of overfitting.

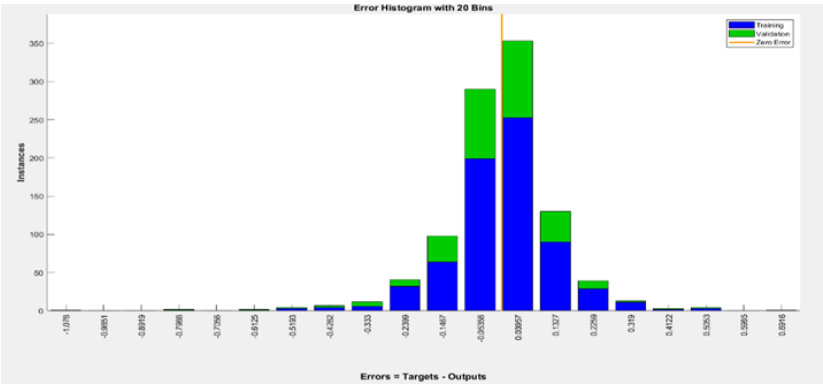

Fig. 23. Training plot: Error histogram

This Figure 24 presents training performance metrics of a neural network across 21 epochs. The top plot shows the gradient steadily decreasing to 0.00067855, indicating that the model is converging. The middle plot displays the learning rate parameter (mu), which quickly stabilizes at 0.0001 after an initial adjustment. The bottom plot shows the validation error (in log scale) increasing slightly after epoch 15, leading to 6 validation checks, which typically triggers early stopping to prevent overfitting. Overall, the training appears stable and well-regularized, with convergence reached by epoch 21.

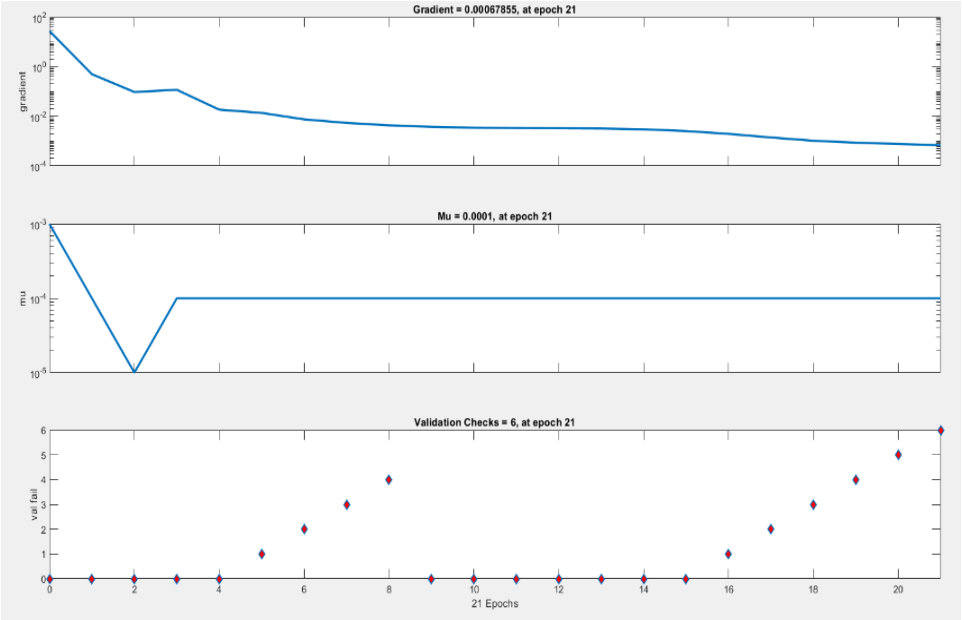

Fig. 24. Training plot: Training states

3.3 Financial feasibility

The economic modeling of the PREC-Fenton system includes estimations of initial investment, capital expenditure (CAPEX), annual operational costs (OPEX), and other relevant economic parameters. In addition, input data for the financial feasibility study of the PREC-Fenton project—such as projected revenue, expenditures, financing structure, and asset salvage value—are presented in detail in Table 7 below. This analysis provides a

foundation for comprehensively evaluating the project's sustainability and profitability potential.

Table 7. Input data for the financial feasibility study of the PREC-Fenton system

Revenue			
TW Production Years 1–10	15,000	ton	
TW Production Years 11–20	13,500	ton	
TW Selling Price	0.006	$./kg	
Revenue Years 1–10	90,000	$./year	
Revenue Years 11–20	81,000	$./year	
Salvage Value	16,929	$.	
Cost			
Plant Capacity	15,000	ton/year	
CAPEX (Capital Expenditure)	0.02	$./kg	
Total Investment Cost	338,575	$.	
MRC (Maintenance and Replacement Cost)	8,145	$./year	with annual inflation
OPEX (Operating Expenditure)	6,772	$./year	with annual inflation
General			
Interest Rate (MARR – Minimum Attractive Rate of Return)	15%	Per year	
Plant Lifetime	20	per year	
Depreciation Period	20		
Depreciation Cost	16,082		
Income Tax	25%		
Inflation	1.84%		
Financing			
Equity Share	30%		
Debt Share	70%		
Net Equity	101,573	$.	
Net Debt	237,003	$.	
Loan Payback Period	10	year	
Loan Interest Rate	6%	Per-year	

3.3.1 Break-even point analysis

The break-even point (BEP) is reached at 44% of production capacity (6,666 tons out of a total of 15,000 tons per year). An increase in capacity by 36% beyond the BEP generates an additional profit of USD 8,000 per year. The visualization is presented in Figure 25 below, and the BEP calculation relative to production capacity is shown in Table 8 below.

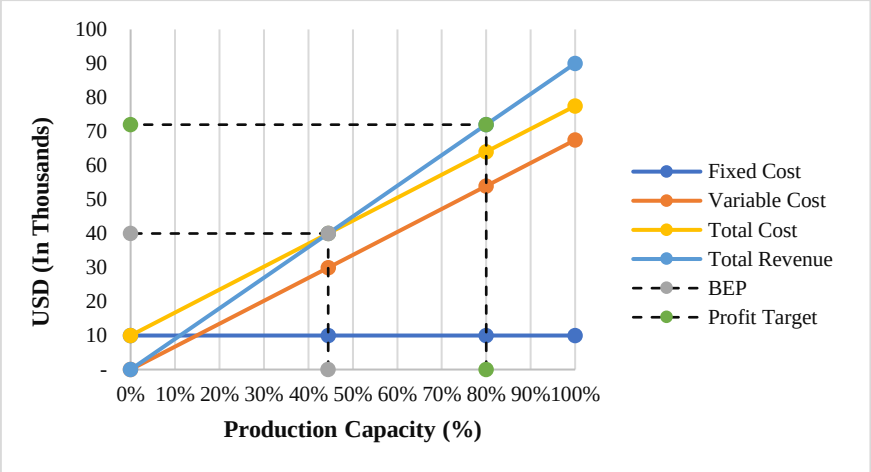

Fig. 25. Break-even point (BEP) graph based on production capacity

Table 8. Break-even point (BEP) calculation of the PREC-Fenton system

Variable	Total cost	Unit
Fixed Cost	10,000	$
Variable Cost	0.005	$/kg
Planned Selling Price	0.006	$/kg
Break-Even Point (in units)	6,666,667	kg
Break-Even Point (in USD)	40,000	$
Target Profit	8,000	$
Units Required to Sell	12,000,000	kg
Sales	72,000	$
Fixed Cost	10,000	$
Variable Cost	54,000	$
Profit	8,000	$
Total Capacity (20 Years)	15,000,000	kg

Unit	Fixed Cost	Variable Cost	Total Cost	Total Revenue
0%	10,000	-	10,000	-
44%	10,000	30,000	40,000	40,000
80%	10,000	54,000	64,000	72,000
100%	10,000	67,500	77,500	90,000

3.3.2 Sensitivity analysis on NPV and IRR

Sensitivity analysis was conducted to identify several key variables. The simulation results indicate that selling price and CAPEX are the most sensitive variables affecting NPV and IRR. Pricing strategy plays a crucial role in maintaining profitability. The calculated sensitivity results for NPV and IRR are presented in Appendix 2 and Appendix 3 below, while the visual representation of the sensitivity analysis is shown in Figure 26 for NPV and Figure 27 for IRR.

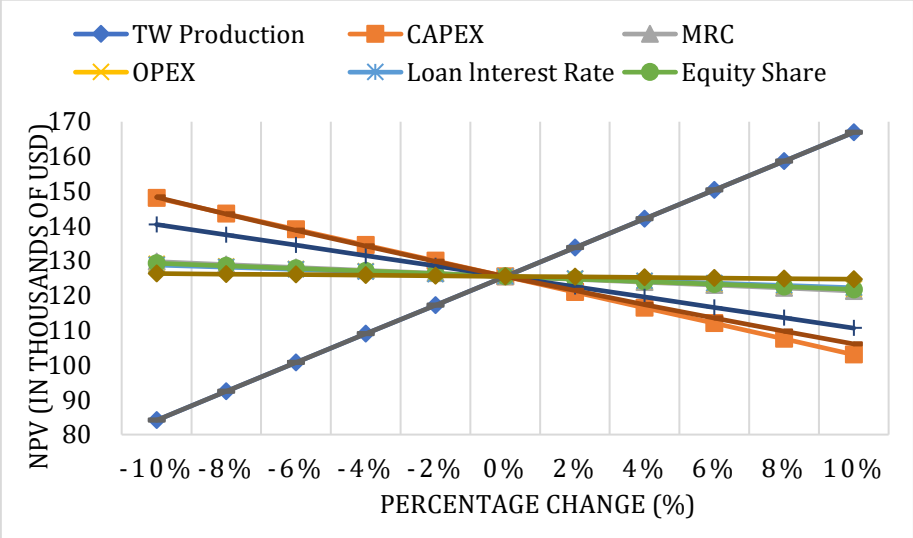

Fig. 26. NPV sensitivity analysis graph

The IRR Sensitivity Analysis chart shows how changes in various parameters affect the Internal Rate of Return (IRR). Among all variables, Selling Price (grey line) has the most significant positive impact—an increase of 10% in selling price leads to an IRR close to 40%, while a 10% decrease reduces IRR to around 28%. Conversely, CAPEX (orange line) shows the strongest negative sensitivity—higher capital expenditures sharply reduce IRR. Other variables like TW Production, MRC, and OPEX have moderate effects, while parameters such as Loan Interest Rate, Equity Share, Debt Share, MARR, and Inflation have relatively minor influence on IRR. The analysis helps identify which factors most critically impact project profitability.

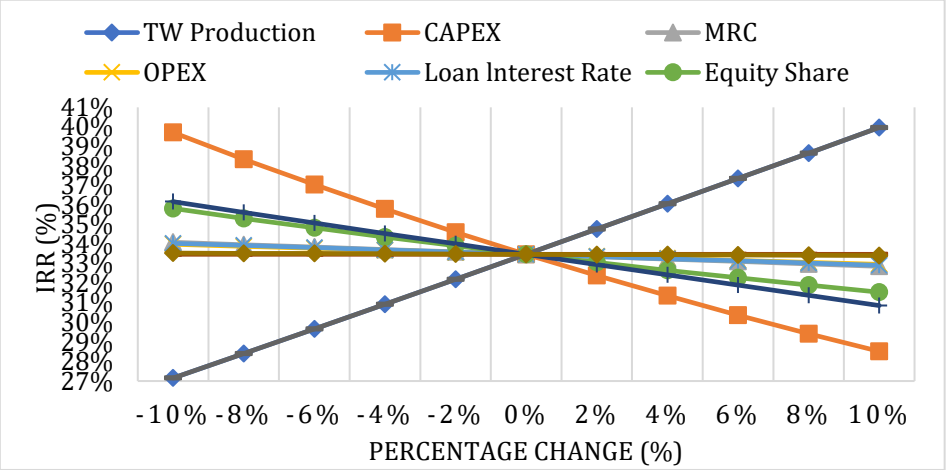

Fig. 27. IRR sensitivity analysis graph

3.3.3 Cash flow analysis

During the project's operational period (20 years), the cash flow remains stable, with an annual depreciation of USD 16,082 and a salvage value of USD 16,929. The complete cash flow diagram is presented in Figure 28 below.

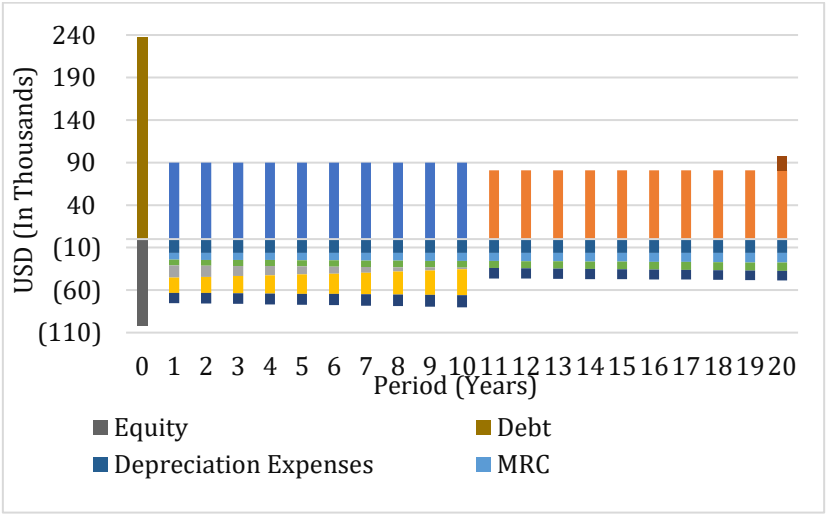

Fig. 28. Cash flow diagram

3.3.4 Key parameter analysis

Based on the results of the financial evaluation, the project demonstrates strong feasibility indicators and holds promising potential for industrial-scale implementation. The Net Present Value (NPV) was recorded at USD 125,529, reflecting a substantial net gain over the project's operational lifespan. This figure confirms that the incoming cash flows exceed both the investment and operational costs. Meanwhile, the Internal Rate of Return (IRR) reached 33.48%, significantly surpassing the Minimum Acceptable Rate of Return (MARR) of 15%, indicating a highly attractive investment return for potential stakeholders.

Table 11. Financial feasibility study results of the PREC-Fenton system

Parameters	Calculated	Requirements	Criteria
Internal Rate of Return (IRR)	33.48%	15%	meet the criteria
Discounted Payback Period (DPP)	5	10	meet the criteria
Net Present Value (NPV)	125,529	+	meet the criteria
Break-Even Point (BEP)	44%	50%	meet the criteria

Additionally, the Discounted Payback Period (DPP) reveals that the initial capital investment can be recovered within five years—well ahead of the planned 20-year operational period (Indrawan et al., 2020; Peng et al., 2021; Wassie & Ahlgren, 2023). These three key financial indicators consistently affirm that the project is not only financially viable but also offers high efficiency and long-term profit potential. Further details of the feasibility study and financial calculations are provided in Table 11 and Table 12.

Tabel 12. Economic parameter sensitivity analysis of the PREC-Fenton system

Sensitivity Analysis	-10%	10%	2%
TW Production	13,500	16,500	300.00
Capital Expenditure (CAPEX)	304,718	372,433	6,772
Minimum Required Cost (MRC)	7,330	8,959	163
Operating Expenditure (OPEX)	6,094	7,449	135
Loan Interest Rate	5.40%	6.60%	0.12%
Equity Share	27.00%	33%	0.60%
Debt Share	63.00%	77%	1.40%
Minimum Acceptable Rate of Return (MARR)	13.50%	17%	0.30%
Selling Price (USD)	0.00540	0.00660	0.00012
Inflation Rate	1.66%	2.02%	0.04%

4. Conclusions

This study successfully developed a PREC-Fenton model that outperforms conventional methods for hazardous waste (B3) treatment, achieving a POP degradation efficiency of up to 99.99%, equivalent to 1,038.8 kg/hour, while producing 176.24 kg/hour of clean water. The system operates with an electro-Fenton potential of 2.13 V across 30 cell units, a hydrogen production rate of 0.83 mol $H_2/m^2 \cdot h$, a membrane surface area of 123.45 m^2, a pumping power of 0.00035 W/m^2, and regeneration heat of 0.054 kW. Integration with an Organic Rankine Cycle (ORC) improves energy efficiency from 40% to 46.13%, yielding a total energy output of 300.17 kW.

System optimization using an Artificial Neural Network (ANN) with an optimal configuration of 13 neurons in a single hidden layer resulted in the lowest RMSE values (0.4838 for the training set and 0.5160 for the validation set) and high R^2 values for K_P, K_I, and K_D parameters at 0.96594, 0.96529, and 0.96753, respectively. The financial feasibility analysis shows that the system is economically viable, with a Net Present Value (NPV) of USD 125,529, an Internal Rate of Return (IRR) of 33.48%, and a Break-Even Point (BEP) of 44%. With these outcomes, the PREC-Fenton system directly contributes to the achievement of SDGs 6, 7, 9, 12, 13, 14, and 15, which are related to clean water and pollution reduction, clean energy, technological innovation, sustainable waste management, environmental impact mitigation, and the preservation of terrestrial and aquatic ecosystems. Therefore, the PREC-Fenton process represents an efficient, economical, and environmentally friendly solution for hazardous waste treatment, aligning with the vision of Smart Society 5.0.

The effectiveness of the PREC-Fenton system can be further enhanced through pilot-scale industrial trials to ensure stability and efficiency under real operational conditions. Additionally, the use of Artificial Neural Networks (ANN) as a fitting tool for PID controller parameters should be reassessed by taking into account the flexibility requirements of industrial applications. Further research is also needed to expand the application of the PREC-Fenton system to various types of hazardous waste (B3), thereby achieving broader and more measurable pollutant reduction impacts.

Acknowledgement

The authors would like to express sincere gratitude to the editorial team and reviewers for their invaluable contributions to this work. The author also acknowledges those who

assisted with language editing, proofreading, and technical writing, which greatly enhanced the quality of this manuscript.

Author Contribution
All authors contributed equally to the conception, design, analysis, and writing of this manuscript.

Funding
This research received no external funding.

Ethical Review Board Statement
Not available.

Informed Consent Statement
Not available.

Data Availability Statement
Not available.

Conflicts of Interest
The authors declare no conflict of interest.

Open Access

References
Abdolrasol, M. G., Hussain, S. S., Ustun, T. S., Sarker, M. R., Hannan, M. A., Mohamed, R., ... & Milad, A. (2021). Artificial neural networks based optimization techniques: A review. *Electronics*, *10*(21), 2689. https://doi.org/10.3390/electronics10212689

Akhtar, A. B. T., Naseem, S., Yasar, A., & Naseem, Z. (2021). Persistent organic pollutants (POPs): sources, types, impacts, and their remediation. *Environmental pollution and remediation*, 213-246. https://doi.org/10.1007/978-981-15-5499-5_8

Balogun, A. L., Marks, D., Sharma, R., Shekhar, H., Balmes, C., Maheng, D., ... & Salehi, P. (2020). Assessing the potentials of digitalization as a tool for climate change adaptation and sustainable development in urban centres. *Sustainable Cities and Society*, *53*, 101888. https://doi.org/10.1016/j.scs.2019.101888

Belalcázar-Saldarriaga, A., Prato-Garcia, D., & Vasquez-Medrano, R. (2019). Photo-Fenton processes in raceway reactors: Technical, economic, and environmental implications during treatment of colored wastewaters. *Journal of Cleaner Production*, *182*, 818–829. https://doi.org/10.1016/j.jclepro.2018.02.058

Bestwick, T., & Camarda, K. V. (2023). Artificial Neural Network-Based Real-Time PID Controller Tuning. *Computer Aided Chemical Engineering, 52*, 1609–1614. https://doi.org/10.1016/B978-0-443-15274-0.50256-0

Bevacqua, M., Tamburini, A., Papapetrou, M., Cipollina, A., Micale, G., & Piacentino, A. (2017). Reverse electrodialysis with NH_4HCO_3-water systems for heat-to-power conversion. *Energy, 137*, 1293–1307. https://doi.org/10.1016/j.energy.2017.07.012

Chen, Q., Lü, F., Zhang, H., & He, P. (2023). Where should Fenton go for the degradation of refractory organic contaminants in wastewater? *Water Research*, *229*, 119479. https://doi.org/10.1016/j.watres.2022.119479

Dapaah, M. F., Niu, Q., Yu, Y.-Y., You, T., Liu, B., & Cheng, L. (2022). Efficient persistent organic pollutant removal in water using MIL-metal–organic framework driven Fenton-like reactions: A critical review. *Chemical Engineering Journal*, *431*, 134182. https://doi.org/10.1016/j.cej.2021.134182

Deb, A., Rumky, J., & Sillanpää, M. (2023). Fenton, Photo-Fenton, and Electro-Fenton Systems for Micropollutant Treatment Processes. In M. Khalid, Y. Park, R. R. Karri, & R. Walvekar. *Advanced Oxidation Processes for Micropollutant*. CRC Press. https://doi.org/10.1201/9781003247913-8

Devi, N. L. (2020). Persistent organic pollutants (POPs): environmental risks, toxicological effects, and bioremediation for environmental safety and challenges for future research. *Bioremediation of Industrial Waste for Environmental Safety: Volume I: Industrial Waste and Its Management*, 53-76. https://doi.org/10.1007/978-981-13-1891-7_4

Dubowski, Y., Alfiya, Y., Gilboa, Y., Sabach, S., & Friedler, E. (2024). A combined approach of electrodialysis pretreatment and vacuum UV for removing micropollutants from natural waters. *Water Research*, *251*, 121152. https://doi.org/10.1016/j.watres.2024.121152

Eisenmenger, N., Pichler, M., Krenmayr, N., Noll, D., Plank, B., Schalmann, E., ... & Gingrich, S. (2020). The Sustainable Development Goals prioritize economic growth over sustainable resource use: a critical reflection on the SDGs from a socio-ecological perspective. *Sustainability Science*, *15*(4), 1101-1110. https://doi.org/10.1007/s11625-020-00813-x

Foteinis, S., Monteagudo, J. M., Durán, A., & Chatzisymeon, E. (2019). Environmental sustainability of the solar photo-Fenton process for wastewater treatment and pharmaceuticals mineralization at semi-industrial scale. *Science of The Total Environment*, *612*, 605–612. https://doi.org/10.1016/j.scitotenv.2017.08.277

George, A. S., & George, A. H. (2024). Towards a Super Smart Society 5.0: Opportunities and Challenges of Integrating Emerging Technologies for Social Innovation. *Partners Universal International Research Journal*, *3*(2), 01-29. https://doi.org/10.5281/zenodo.11522048

Getachew Gizaw, D., Periyasamy, S., Senthil Kumar, P., Salilih, E. M., Redda, Z. T., Velusamy, K., & Rangasamy, G. (2023). Artificial neural network based identification of process dynamics and neural network controller design for continuous distillation column. *Sustainable Energy Technologies and Assessments*, *57*, 103168. https://doi.org/10.1016/j.seta.2023.103168

Giacalone, F., Vassallo, F., Scargiali, F., Tamburini, A., Cipollina, A., & Micale, G. (2020). The first operating thermolytic reverse electrodialysis heat engine. *Journal of Membrane Science*, *595*, 117522. https://doi.org/10.1016/j.memsci.2019.117522

Hajiali, M., Farhadian, M., & Tangestaninejad, S. (2022). Enhance performance ZnO/ Bi2MoO6/ MIL-101(Fe) grown on fluorine-doped tin oxide as photoanode and CuO/ Cu2O based on Cu mesh photocathode in the photocatalytic fuel cell. *Energy Conversion and Management*, *269*, 116137. https://doi.org/10.1016/j.enconman.2022.116137

Hamedani, E. A., Abasalt, A., & Talebi, S. (2024). Application of microbial fuel cells in wastewater treatment and green energy production: a comprehensive review of technology fundamentals and challenges. *Fuel*, *370*, 131855. https://doi.org/10.1016/j.fuel.2024.131855

Hariram, N. P., Mekha, K. B., Suganthan, V., & Sudhakar, K. (2023). Sustainalism: An integrated socio-economic-environmental model to address sustainable development

and sustainability. *Sustainability*, *15*(13), 10682. https://doi.org/10.3390/su151310682

Hassan, M., Kanwal, S., Singh, R. S., SA, M. A., Anwar, M., & Zhao, C. (2024). Current challenges and future perspectives associated with configuration of microbial fuel cell for simultaneous energy generation and wastewater treatment. *International Journal of Hydrogen Energy*, *50*, 323-350. https://doi.org/10.1016/j.ijhydene.2023.08.134

Hassan, M., Liu, Y., Naidu, R., Du, J., & Qi, F. (2020). Adsorption of Perfluorooctane sulfonate (PFOS) onto metal oxides modified biochar. *Environmental Technology & Innovation*, *19*, 100816. https://doi.org/10.1016/j.eti.2020.100816

Indrawan, N., Simkins, B., Kumar, A., & Huhnke, R. L. (2020). Economics of distributed power generation via gasification of biomass and municipal solid waste. *Energies*, *13*(14), 3703. https://doi.org/10.3390/en13143703

Jiménez-Bambague, E. M., Madera-Parra, C. A., Rangel-Delgado, M. F., Quintero- Martinez, I., Miranda-Mosquera, D., Aristizabal-Apolinar, J. S., & Machuca-Martínez, F. (2023). Photo-Fenton and Electro-Fenton performance for the removal of pharmaceutical compounds in real urban wastewater. *Electrochimica Acta*, *442*, 141905. https://doi.org/10.1016/j.electacta.2023.141905

Kasinathan, P., Pugazhendhi, R., Elavarasan, R. M., Ramachandaramurthy, V. K., Ramanathan, V., Subramanian, S., ... & Alsharif, M. H. (2022). Realization of sustainable development goals with disruptive technologies by integrating industry 5.0, society 5.0, smart cities and villages. *Sustainability*, *14*(22), 15258. https://doi.org/10.3390/su142215258

Kim, D.-H., Lee, H., Kim, K., Kim, S., Kim, J. H., Ko, Y. W., Hawes, I., Oh, J.-E., & Kim, J.-T. (2024). Persistent organic pollutants in the Antarctic marine environment: The influence impacts of human activity, regulations, and climate change. *Environmental Pollution*, *363*, 125100. https://doi.org/10.1016/j.envpol.2024.125100

Kumar, R., Singh, L., Zularisam, A. W., & Hai, F. I. (2018). Microbial fuel cell is emerging as a versatile technology: a review on its possible applications, challenges and strategies to improve the performances. *International Journal of Energy Research*, *42*(2), 369-394. https://doi.org/10.1002/er.3780

Kwon, K., Park, B. H., Kim, D. H., & Kim, D. (2015). Parametric study of reverse electrodialysis using ammonium bicarbonate solution for low-grade waste heat recovery. *Energy Conversion and Management, 103*, 104–110. https://doi.org/10.1016/j.enconman.2015.06.051

Leng, Q., Li, F., Tao, Z., Wang, Z., & Wu, X. (2024). Advanced Wastewater Treatment: Synergistic Integration of Reverse Electrodialysis with Electrochemical Degradation Driven by Low-Grade Heat. *Energies*, *17*(21), 5362. https://doi.org/10.3390/en17215362

Leng, Q., Xu, S., Wu, X., Wang, S., Jin, D., Wang, P., Wu, D., & Dong, F. (2022). Degrade Methyl Orange by a Reverse Electrodialysis Reactor Coupled with Electrochemical Direct Oxidation and Electro-Fenton Processes. *Electrocatalysis*, *13*(3), 242–254. https://doi.org/10.1007/s12678-022-00712-y

Machado, F., Teixeira, A. C. S. C., & Ruotolo, L. A. M. (2023). Critical review of Fenton and photo-Fenton wastewater treatment processes over the last two decades. *International Journal of Environmental Science and Technology*, *20*(12), 13995–14032. https://doi.org/10.1007/s13762-023-05015-3

Mandal, A., Senthil Kumar, P., Poorva, C. S., Srinivasa Raju, L., Balasubramani, S. R., & Rangasamy, G. (2024). Research progress of persistent organic pollutants in water: Classification, sources, potential risks, and treatment approaches. *Water Practice & Technology*, *19*(3), 937–959. https://doi.org/10.2166/wpt.2024.031

Mardani, M. M., Lazar, R. D., Mijatovic, N., & Dragičević, T. (2022). Artificial neural network-based constrained predictive real-time parameter adaptation controller for grid-tied VSCs. *IEEE Journal of Emerging and Selected Topics in Power Electronics*, *11*(2), 1507-1517. https://doi.org/10.1109/JESTPE.2022.3214342

Matesun, J., Petrik, L., Musvoto, E., Ayinde, W., & Ikumi, D. (2024). Limitations of wastewater treatment plants in removing trace anthropogenic biomarkers and future directions: A review. *Ecotoxicology and Environmental Safety*, *281*, 116610. https://doi.org/10.1016/j.ecoenv.2024.116610

Mishra, A., Kumari, M., Kumar, R., Iqbal, K., & Thakur, I. S. (2022). Persistent organic pollutants in the environment: Risk assessment, hazards, and mitigation strategies. *Bioresource Technology Reports*, *19*, 101143. https://doi.org/10.1016/j.biteb.2022.101143

Moallemi, E. A., Malekpour, S., Hadjikakou, M., Raven, R., Szetey, K., Ningrum, D., ... & Bryan, B. A. (2020). Achieving the sustainable development goals requires transdisciplinary innovation at the local scale. *One Earth*, *3*(3), 300-313. https://doi.org/10.1016/j.oneear.2020.08.006

Peng, C. Y., Kuo, C. C., & Tsai, C. T. (2021). Optimal configuration with capacity analysis of PV-PLUS-BESS for behind-the-meter application. *Applied Sciences*, *11*(17), 7851. https://doi.org/10.3390/app11177851

Pizzorno, J. E., & Murray, M. T. (Eds.). (2021). *Textbook of natural medicine* (Fifth edition). Elsevier.

Raka, Y. D., Karoliussen, H., Lien, K. M., & Burheim, O. S. (2020). Opportunities and challenges for thermally driven hydrogen production using reverse electrodialysis system. *International Journal of Hydrogen Energy, 45*(2), 1212–1225. https://doi.org/10.1016/j.ijhydene.2019.05.126

Ramírez-Márquez, C., Posadas-Paredes, T., Raya-Tapia, A. Y., & Ponce-Ortega, J. M. (2024). Natural resource optimization and sustainability in society 5.0: A comprehensive review. *Resources*, *13*(2), 19. https://doi.org/10.3390/resources13020019

Ranade, A., Singh, K., Tamburini, A., Micale, G., & Vermaas, D. A. (2022). Feasibility of producing electricity, hydrogen, and chlorine via reverse electrodialysis. *Environmental Science & Technology, 56*(22), 16062–16072. https://doi.org/10.1021/acs.est.2c03407

Rokni, L., Rezaei, M., Rafieizonooz, M., Khankhajeh, E., Mohammadi, A. A., & Rezania, S. (2023). Effect of Persistent Organic Pollutants on Human Health in South Korea: A Review of the Reported Diseases. *Sustainability*, *15*(14), 10851. https://doi.org/10.3390/su151410851

Seborg, D. E., Edgar, T. F., Mellichamp, D. A., & Doyle III, F. J. (2020). *Process Dynamics and Control* (4th ed.). Hoboken, NJ: John Wiley & Sons.

Smara, M., Khalladi, R., Moulai-Mostefa, N., Madi, K., Mansour, D., Lekmine, S., Benslama, O., Tahraoui, H., Zhang, J., & Amrane, A. (2024). Efficiency of hydrogen peroxide and Fenton reagent for polycyclic aromatic hydrocarbon degradation in contaminated soil: Insights from experimental and predictive modeling. *Processes, 12*(3), 621. https://doi.org/10.3390/pr12030621

Tarascon, J.-M., & Simon, P. (2015). *Electrochemical energy storage*. John Wiley & Sons. https://doi.org/10.1002/9781118998151

Thakur, A. K., & Malmali, M. (2022). Advances in polymeric cation exchange membranes for electrodialysis: An overview. *Journal of Environmental Chemical Engineering*, *10*(5), 108295. https://doi.org/10.1016/j.jece.2022.108295

Tian, H., & Wang, Y. (2022). A new photoelectrochemical cell coupled with the Fenton reaction to remove pollutant and generate electricity under the drive of waste heat. *Science of The Total Environment*, *839*, 156277. https://doi.org/10.1016/j.scitotenv.2022.156277

Ukoba, K., Olatunji, K. O., Adeoye, E., Jen, T. C., & Madyira, D. M. (2024). Optimizing renewable energy systems through artificial intelligence: Review and future prospects. *Energy & Environment*, *35*(7), 3833-3879. https://doi.org/10.1177/0958305X241256293

Wang, N., Sun, X., Zhao, Q., & Wang, P. (2021). Treatment of polymer-flooding wastewater by a modified coal fly ash-catalysed Fenton-like process with microwave pre-

enhancement: System parameters, kinetics, and proposed mechanism. *Chemical Engineering Journal*, *406*, 126734. https://doi.org/10.1016/j.cej.2020.126734

Wassie, Y. T., & Ahlgren, E. O. (2023). Long-term optimal capacity expansion planning for an operating off-grid PV mini-grid in rural Africa under different demand evolution scenarios. *Energy for Sustainable Development*, *76*, 101305. https://doi.org/10.1016/j.esd.2023.101305

Wilailak, S., Yang, J.-H., Heo, C.-G., Kim, K.-S., Bang, S.-K., Seo, I.-H., Zahid, U., & Lee, C.-J. (2021). Thermo-economic analysis of Phosphoric Acid Fuel-Cell (PAFC) integrated with Organic Ranking Cycle (ORC). *Energy, 220*, 119744. https://doi.org/10.1016/j.energy.2020.119744

Xu, W., Xue, W., Huang, H., Wang, J., Zhong, C., & Mei, D. (2021). Morphology controlled synthesis of α-Fe2O3-x with benzimidazole-modified Fe-MOFs for enhanced photo-Fenton-like catalysis. *Applied Catalysis B: Environmental*, *291*, 120129. https://doi.org/10.1016/j.apcatb.2021.120129

Biographies of Authors

Naufal Fawwaz Dienulloh, Department of Chemical Engineering, Faculty of Engineering, Universitas Brawijaya, Malang, East Java, 65145, Indonesia.

- Email: naufalfawwaz@student.ub.ac.id
- ORCID: N/A
- Web of Science ResearcherID: N/A
- Scopus Author ID: N/A
- Homepage: N/A

Rizky Maulana Riadhi, Department of Chemical Engineering, Faculty of Engineering, Universitas Brawijaya, Malang, East Java, 65145, Indonesia.

- Email: rizkymaulanar@student.ub.ac.id
- ORCID: N/A
- Web of Science ResearcherID: N/A
- Scopus Author ID: N/A
- Homepage: N/A

Supriyono, Department of Chemical Engineering, Faculty of Engineering, Universitas Brawijaya, Malang, East Java, 65145, Indonesia.

- Email: supriyono16@ub.ac.id
- ORCID: 0000-0002-2494-1898
- Web of Science ResearcherID: N/A
- Scopus Author ID: 57200566362
- Homepage: https://teknikkimia.ub.ac.id/profil/sumber-daya-manusia/data-dosen-2/supriyono-s-t-m-t/

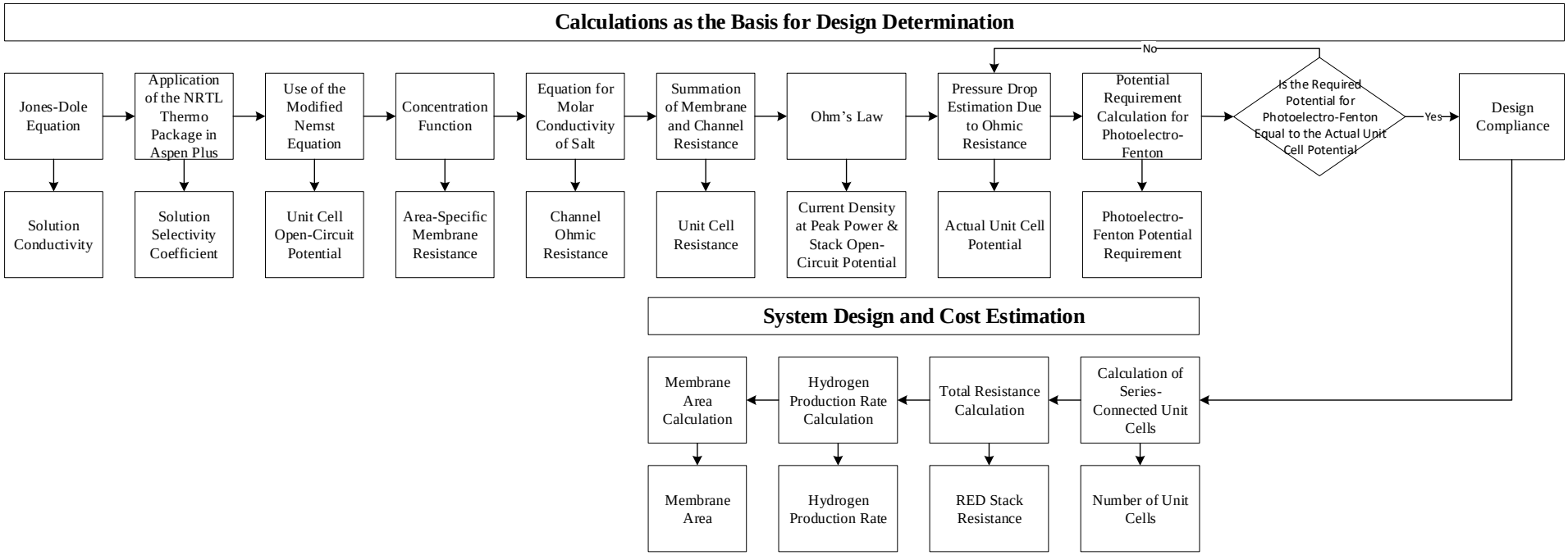

Appendix 1. Aspen plus design inputs

Appendix 2. Sensitivity analysis of economic parameters on net present value (NPV)

Percentage Change	TW Production	CAPEX	MRC	OPEX	Loan lnterest Rate	Equity Share	Debt Share	MARR	Selling Price	Inflation
-10%	84,116	148,074	129,762	129,048	128,770	129,299	140,433	148,291	84,116	126,336
-8%	92,398	143,565	128,916	128,345	128,125	128,545	137,452	143,440	92,398	126,176
-6%	100,681	139,056	128,069	127,641	127,479	127,791	134,472	138,745	100,681	126,015
-4%	108,964	134,547	127,222	126,937	126,831	127,037	131,491	134,198	108,964	125,853
-2%	117,246	130,038	126,376	126,233	126,181	126,283	128,510	129,795	117,246	125,691
0%	125,529	125,529	125,529	125,529	125,529	125,529	125,529	125,529	125,529	125,529
2%	133,811	121,020	124,682	124,825	124,875	124,775	122,548	121,395	133,811	125,366
4%	142,094	116,511	123,836	124,121	124,219	124,021	119,567	117,387	142,094	125,202

6%	150,377	112,002	122,989	123,417	123,561	123,267	116,586	113,502	150,377	125,038
8%	158,659	107,493	122.42	122,713	122,901	122,513	113,605	109,734	158,659	124,874
10%	166,942	102,984	121,296	122,009	122,239	121,759	110,624	106,079	166,942	124,708

Appendix 3. Sensitivity analysis of economic parameters on internal rate of return (IRR)

Percentage Change	TW Production	CAPEX	MRC	OPEX	Loan lnterest Rate	Equity Share	Debt Share	MARR	Selling Price	Inflation
-10%	27.15%	39.72%	34.10%	34.00%	34.04%	35.83%	36.18%	33.48%	27.15%	33.55%
-8%	28.40%	38.35%	33.98%	33.89%	33.93%	35.32%	35.63%	33.48%	28.40%	33.53%
-6%	29.66%	37.05%	33.85%	33.79%	33.82%	34.83%	35.09%	33.48%	29.66%	33.52%
-4%	30.93%	35.80%	33.73%	33.69%	33.71%	34.37%	34.55%	33.48%	30.93%	33.51%
-2%	32.20%	34.62%	33.61%	33.59%	33.60%	33.92%	34.02%	33.48%	32.20%	33.50%
0%	33.48%	33.48%	33.48%	33.48%	33.48%	33.48%	33.48%	33.48%	33.48%	33.48%
2%	34.77%	32.40%	33.36%	33.38%	33.37%	33.07%	32.95%	33.48%	34.77%	33.47%
4%	36.06%	31.37%	33.24%	33.28%	33.26%	32.67%	32.43%	33.48%	36.06%	33.46%
6%	37.36%	30.38%	33.11%	33.18%	33.15%	32.28%	31.90%	33.48%	37.36%	33.45%
8%	38.66%	29.43%	32.99%	33.07%	33.03%	31.91%	31.38%	33.48%	38.66%	33.43%
10%	39.97%	28.52%	32.87%	32.97%	32.92%	31.55%	30.86%	33.48%	39.97%	33.42%